Amplification in Ytterbium-doped fibers

Vasuki Durairaj

School of Electrical Engineering

Thesis submitted for examination for the degree of Master of Science in Technology.
Espoo 24th May 2013

Thesis supervisor:

Hanne Ludvigsen, Docent

Thesis advisor:

Dr. Steffen Novotny

Aalto University
School of Electrical
Engineering

AALTO UNIVERSITY
SCHOOL OF ELECTRICAL ENGINEERING

ABSTRACT OF THE
MASTER'S THESIS

Author: Vasuki Durairaj

Title: Amplification in Ytterbium-doped fibers

Date: 24th May 2013 Language: English Number of pages:10+59

Department of Micro- and Nanosciences

Professorship: Micro- and Nanotechnology Code: S-104

Supervisor: Hanne Ludvigsen, Docent

Advisor: Dr. Steffen Novotny

Fiber lasers and amplifiers are quickly replacing conventional bulk optical devices in a variety of applications. Ytterbium-doped fibers are of particular interest in high power applications due to their numerous advantages arising from a simple electronic structure. The behavior of Ytterbium-doped fiber devices is however strongly influenced by the selection of absorption and emission wavelengths and other parameters. Careful theoretical analysis is required to optimize the performance of the fiber device and to estimate the influence of amplified spontaneous emission, photodarkening and other such phenomena.

The objective of this thesis is to study the amplification process in Ytterbium-doped fibers experimentally and theoretically, as a preliminary step to designing a high power pump source. For this purpose, a fiber laser and an amplifier operating in the continuous wave regime have been experimentally realized based on Ytterbium-doped double-clad fibers in a free-space configuration. Theoretical models of these devices have been simulated using a commercial simulation software.

The influence of various design and fiber parameters on the performance of the devices have been studied in simulations and good agreement between the results for both the fiber laser and amplifier is found.

Keywords: Ytterbium-doped fibers, Double-clad fibers, Fiber amplifiers, Fiber lasers

Acknowledgments

This thesis work has been carried out in the Fiber Optics research group of the Department of Micro- and Nanosciences at Aalto University.

I would like to thank my supervisor Hanne Ludvigsen, for giving me the opportunity to work on this project. I also thank her for her invaluable guidance and support and more importantly, her constant faith in my abilities.

I would also like to extend my deepest gratitude to my mentor Dr. Steffen Novotny, for his patience in educating me on scientific practices and writing skills, and for teaching me the virtue of thoroughness.

My special thanks to Igor Shavrin for his practical advice on everything from cleaning lenses to surviving research work. I wish to also mention my thanks to Alexander Savelyev and Adam Kotrc, whose cheerful company I missed very much during the later part of the thesis work.

Liekki and especially Joan Jesús Montiel i Ponsoda, are thanked for the generous loan of fibers and equipment.

The work has been financially supported by the Academy of Finland as part of the 'Photonics and Modern Imaging Techniques' research programme (Projects: 134857, 134857).

Last but not least, I express my warmest gratitude to my husband, Ajai Iyer, without whom neither life nor learning would have any joy. My humble thanks also to our parents for their support and love.

Otaniemi, 24^{th} May 2013.

Vasuki Durairaj

Contents

List of Figures

List of Tables

Symbols

N_t	Concentration of Ytterbium ions
n_1	Normalized population of Ytterbium ions in ground state
n_2	Normalized population of Ytterbium ions in excited state
R_{12}	Pump excitation rate
R_{21}	Pump de-excitation rate
W_{12}	Seed absorption rate
W_{21}	Seed emission rate
A_{21}	Spontaneous emission rate
τ	Fluorescence life time of Yb^{3+} ions
h	Planck's constant
ν_p	Pump frequency
ν_s	Seed frequency
λ_p	Pump wavelength
λ_s	Seed wavelength
Γ_p	Overlap factor of pump mode field with doped area
Γ_s	Overlap factor of seed mode field with doped area
I_p	Pump intensity
I_s	Seed intensity
A	Effective core area
S_d	Cross-section area of doped region
S_{ic}	Cross-section area of inner-cladding
S_c	Cross-section area of core
σ_{ep}	Emission cross-section at pump wavelength
σ_{ap}	Absorption cross-section at pump wavelength
σ_p	$\sigma_{ep} + \sigma_{ap}$
σ_{es}	Emission cross-section at seed wavelength
σ_{as}	Absorption cross-section at seed wavelength
σ_s	$\sigma_{es} + \sigma_{as}$
R	Reflectivity
T	Transmissivity
L	Fiber length
α	Absorption co-efficient

Abbreviations

EDFA	Erbium-doped fiber amplifier
YDFL	Ytterbium-doped fiber laser
YDFA	Ytterbium-doped fiber amplifier
NA	Numerical aperture
DC	Double clad
LMA	Large mode-area
PCF	Photonic crystal fiber
CW	Continuous wave
ASE	Amplified spontaneous emission
ESA	Excited state absorption
GVD	Group velocity dispersion
MOPA	Master oscillator power amplifier
NLSE	Nonlinear Schrödinger equation
FWHM	Full-width half-maximum
DCM	Dichroic mirror
BPF	Band pass filter
LPF	Long pass filter
LD	Laser diode
PM	Polarization maintaining
FBG	Fiber Bragg grating

1 Introduction

The concept of using fiber waveguide structures as optical gain media was first proposed by Snitzer *et al.* as early as 1961 [1]. Potential single mode operation was the main reason for interest in fiber based optical systems since it would enable excellent beam quality. In 1964, only three years after the proposal, a Neodymium(Nd)-doped glass fiber laser [2] and a pulsed optical amplifier side-pumped by a flash tube [3] were demonstrated. Though single mode guidance was the initial motivation, fiber fabrication technologies and pump sources available at that time enabled the realization of only multimode fiber devices [3–5]. It took almost two decades for these technologies to advance sufficiently enough to make practical realization of single mode fiber systems feasible. The first single-mode fiber laser was demonstrated by Mears *et al.* in 1985 [6] using Nd-doped low-loss silica fibers.

Neodymium was the dopant of interest in initial years due to the high power and efficiency of the 1060 nm transition and availability of Nd-doped crystalline and bulk glass laser sources. The success of Nd-doped fiber lasers and development of simple rare-earth doping procedures in low-loss silica fibers reported in [7,8], led to further investigation of other rare-earth-doped fibers. In 1987, Erbium(Er)-doped single mode fiber amplifiers were first demonstrated simultaneously by Payne *et al.*, from the University of Southampton [9] and Desurvire *et al.*, from AT&T Bell Laboratories [10]. This marked the beginning of an era of increased interest in fiber devices and rapid growth of fiber technologies, owing mainly to the operating wavelength of Er-doped fiber amplifiers (EDFA), which lies in the telecommunication wavelength region (1.55 μm).

Need for higher output powers and growth of fiber-based applications beyond the telecommunication industry, triggered the study of other rare earth dopants such as Thulium (Tm), Ytterbium (Yb), Praseodymium (Pr) and Holmium (Ho).

Ytterbium-doped fibers in particular, were found to have a number of advantages due to their distinctive electronic structure, which favors their use in high power laser systems. In 1988, Hanna *et al.* demonstrated a Ytterbium-doped fiber laser (YDFL) [11], pumped by a dye laser operating at 840 nm. Continuous advancements in fiber technologies have led to realization of very high power fiber lasers and two decades after their first demonstration, YDFLs with multi-kW single mode outputs were demonstrated [12] with a possibility for even further scaling.

Power-scaling, however, leads to the onset of various nonlinear effects and thermal effects in the fibers. Mechanisms such as quenching and photo-darkening are not yet fully understood. Detailed theoretical studies have become inevitable in order to fully understand such parameters and to design efficient fiber devices. Though modeling of Yb-doped fiber systems has received increased interest recently [13–19], development and implementation of such theoretical models for complex systems are typically difficult and time consuming for those not in the field of fiber optics. Growing popularity and diversity of fiber amplifier and laser applications has increased the need for simple but powerful simulation tools which would enable flexible modeling of fiber devices for understanding and design of such systems. Commercial simulation tools have thus begun to emerge in the recent years.

The motivation for this thesis is the design and implementation of a multi-stage high-power pump source based on Ytterbium-doped fibers. As a preliminary phase, the amplification process in Ytterbium-doped fibers is studied experimentally and theoretically in this thesis. A fiber laser and an amplifier operating in the continuous wave regime are experimentally realized using Ytterbium-doped double-clad fibers. The devices are also theoretically modeled using a commercial simulation software and the influence of various fiber parameters and design considerations are studied in simulations.

The work is organized in six chapters. The principles of fiber amplifiers and lasers are presented in Chapter 2 along with the background information regarding the unique properties of Ytterbium-doped gain media and the development of fiber laser technology. The theory of modeling Ytterbium-doped fiber devices is discussed in Chapter 3 and the performance of the simulation tool is analyzed in comparison with a simple theoretical model. The experimental amplifier and laser designs are explained in Chapter 4 and the measurement results are presented. In Chapter 5, the measurements are compared to the simulated outputs and the effects of various simulation parameters are discussed. The results and observations are summarized in Chapter 6.

2 Ytterbium-doped fiber devices

The principles and characteristics of Ytterbium-doped fiber devices are presented in this chapter. The chapter is organized in the following manner: The principles of laser and a brief history of the development of rare-earth doped fiber amplifiers and lasers are presented in the first section. Developments in fiber technologies which enabled the power scaling of fiber devices are briefly discussed in the second section. The noise, nonlinearities and other detrimental effects occurring in high power fiber devices are explained in the third section. Finally, the specific properties and characteristics of Ytterbium-doped fibers which make them highly attractive for high power fiber applications are discussed in detail in the fourth section.

2.1 Laser principles

The three main processes occurring in an optically active medium due to interaction of light and matter are (1) absorption (2) spontaneous emission and (3) stimulated emission. A simplified schematic of these processes when only two energy levels E_1 and E_2, are involved is shown in Fig. 2.1.

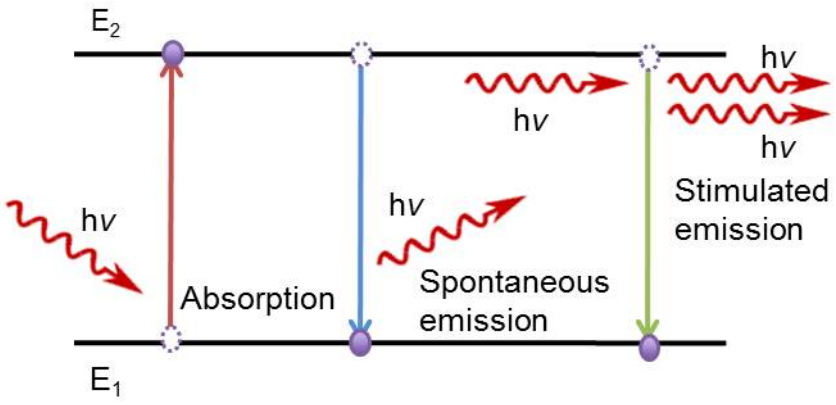

Figure 2.1: Schematic of absorption, spontaneous emission and stimulated emission in a two-level system.

Consider an atomic or molecular medium whose electrons are in ground-state E_1. When a photon of frequency ν with energy E given by Eq. 1,

$$E = h\nu = E_2 - E_1 \tag{1}$$

is incident on such medium, the energy is transferred to the electrons which are then excited to a higher energy level E_2. This process is called absorption and it

can result in population inversion, which is the state where more electrons exist in the excited energy level compared to the ground level.

The excited electrons can return to the ground-state without the influence of an external electromagnetic field, by emission of a photon. This process is referred to as spontaneous emission or luminescence. Spontaneous emission generally occurs in all direction, resulting in spatially incoherent radiation.

In contrast, when a photon of energy E interacts with the excited electron, a process equal but opposite to absorption occurs. This results in the emission of an additional photon with similar phase, frequency, polarization and direction of travel as that of the incident photon. This process is known as stimulated emission. The theory of stimulated emission was first described by Einstein in 1917 [20]. When a medium is prepared in a state of population inversion by pumping and an optical feedback is provided by a resonator cavity, the stimulated emission can be amplified to yield a highly coherent beam of light.

The first experimental device realizing the concepts of population inversion and stimulated emission was reported in 1954 [21]. In this demonstration, ammonia (NH_3) molecules were used to achieve emission in the microwave region. In 1958, Schawlow and Townes [22] proposed a system for stimulated emission at infrared and optical wavelengths and soon after, the first solid-state laser operating at optical wavelengths was demonstrated in a ruby crystal in 1960 [23].

A typical configuration of a solid-state laser is shown in Fig. 2.2. Pump light is focused into a solid laser rod/crystal which is sandwiched between two mirrors. Mirror 1 is chosen to have high reflectivity at laser wavelength and high transmissivity at pump wavelength whereas mirror 2 is partially reflecting to enable output coupling. The dimensions of the laser rod are typically of the order of a few millimeters in diameter and several centimeters in length.

Despite the many advantages, conventional rod lasers face power-dependent thermo-optical problems such as thermal-stress induced birefringence and thermal lensing, which result in poor beam quality at high operating powers. Also, the lack of waveguiding mechanisms in bulk lasers results in a high beam divergence which limits the interaction lengths and consequently the gain of the system.

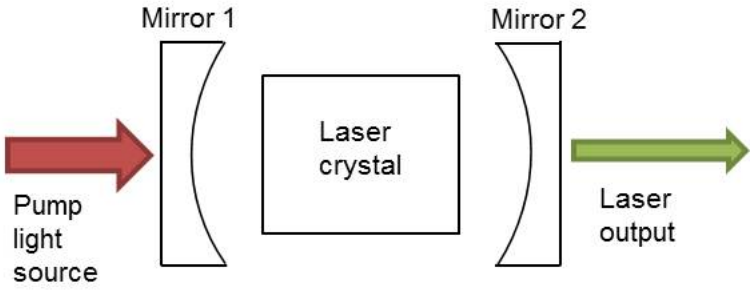

Figure 2.2: Schematic of solid-state laser.

2.2 Rare-earth doped fiber devices

The guidance of light in fibers/rods was first investigated by Heel in 1954 [24]. In this work, total internal reflection occurring in glass and plastic fibers with a high refractive index core surrounded by a lower refractive index cladding was observed. In 1961 [1], Snitzer *et al.* proposed the use of such fiber waveguides as laser cavities for achieving excellent beam quality. Simultaneously, the use of rare-earth ions as dopants also gained interest in the early 1960s when stimulated emission at optical wavelengths was observed from such ions in various host media [25, 26]. Soon these ions were embedded in glass fibers and the first experimental demonstrations of rare-earth-doped fiber laser and amplifier was reported by Snitzer *et al.* in 1964 [2,3].

The lack of suitable pump sources and fiber fabrication techniques, however, posed a number of problems to the development of rare-earth-doped fiber devices was slow in the initial years. Early fiber devices were typically less than two meters long with core diameters of the order of few microns, pumped by flashtubes, dye lasers or injection lasers [5]. These fibers were mostly made from glass which had high losses and hence long fiber lengths were not practical. In 1980s, mainly due to the efforts of Payne *et al.*, significant advancements in fiber doping techniques were achieved [7, 8] and extremely long, low-loss silica fibers were manufactured. Simultaneous advancements in semiconductor laser technology led to the development of continuous wave single-mode diode lasers operating at room temperatures. With availability of uniformly doped, low-loss single-mode fibers and single-mode pump sources, the first single-mode fiber laser operating in continuous wave regime was demonstrated by Mears *et al.* in 1985 [6].

The schematics of a single-clad end-pumped linear-cavity fiber laser and a co-pumped fiber amplifier are shown in Fig. 2.3. The pump and seed light are both confined in the single-mode core by total internal reflection, which results in excellent overlap between pump and seed.

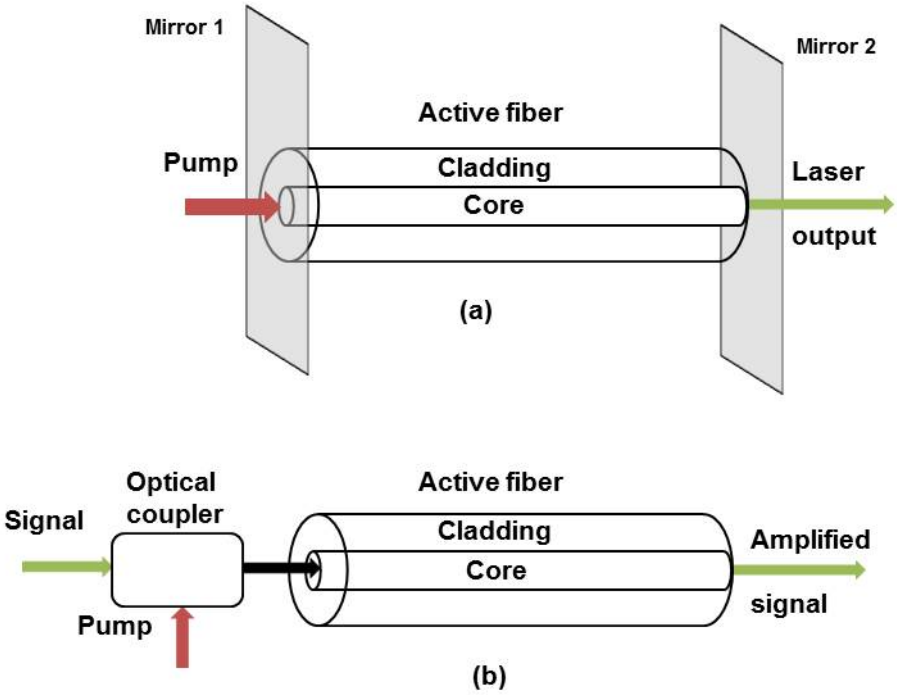

Figure 2.3: Schematic of (a) End-pumped linear-cavity fiber laser and (b)Co-pumped fiber amplifier.

Fiber lasers and amplifiers can be classified into a number of types depending on parameters such as operation regime (continuous wave or pulsed), principle (Raman or upconversion), cavity design (in case of lasers), and pump scheme used.

Laser cavity design

Based on the design of the resonator cavity, fiber lasers are mainly classified into two categories as (1) linear cavity and (2) ring cavity fiber lasers. A linear cavity fiber laser consists of a Fabry-Perot cavity. In the simplest case, this cavity can be formed from the end Fresnel reflections at the fiber facets. For efficient lasing, linear cavities are formed by butt-coupling highly reflecting dielectric mirrors to the fiber facets, or forming fiber Bragg gratings (FBG) at fiber ends or using passive fiber components such as Sagnac loops. In ring-fiber lasers the resonator cavity is typically formed as a loop with passive fibers and couplers to provide uni-directional feedback. Some typical designs of laser resonator cavities are shown in Fig. 2.4.

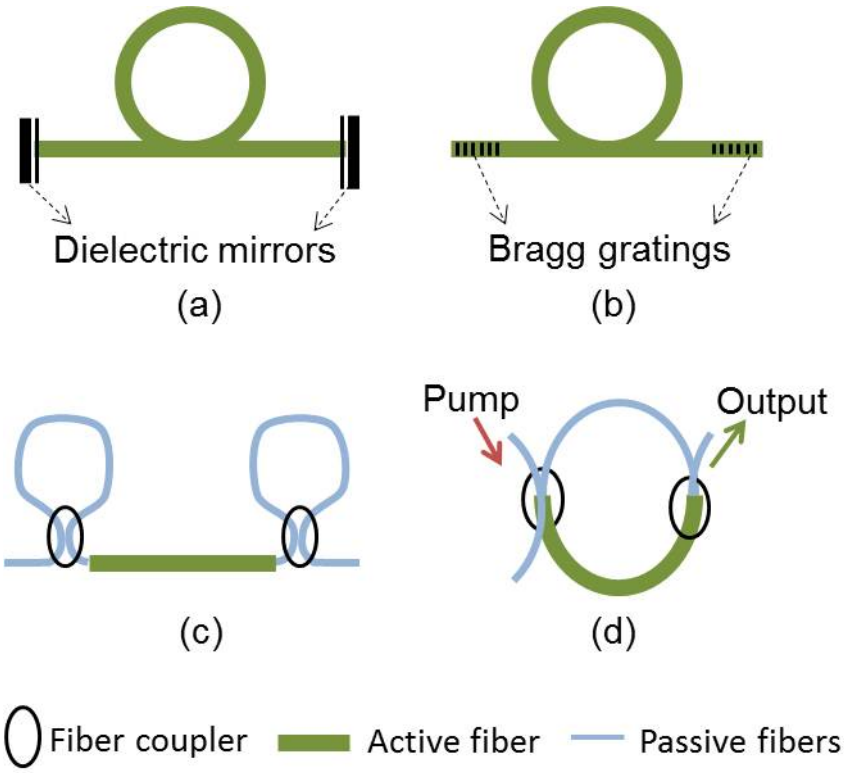

Figure 2.4: Schematics of different laser resonator cavities: Linear cavity lasers using (a) Dielectric mirrors, (b) Bragg gratings, (c) Sagnac loop and (d) Ring cavity laser.

Pump schemes

Another important factor in designing fiber lasers and amplifiers is the pump scheme. Based on the coupling technique, some common pump schemes are side-pumping, end-pumping and V-groove side-pumping. Based on the direction of pump propagation with respect to seed/laser propagation, the pump schemes are classified as counter-pumping, co-pumping and bidirectional-pumping. Optical isolators are used at the input and output ends to protect the seed and pump sources from back-reflections.

2.3 Power scaling

Though single-clad fiber devices can achieve a very high gain, the maximum output power is limited due to the power available from single-mode pump sources. High power pump sources typically have a multi-mode output and hence cannot be used effectively to pump single-clad fibers. This has led to the investigation of various

alternative fiber designs and architectures [27, 28]. Evolution of fiber technologies which enabled power-scaling are discussed in the following subsection.

2.3.1 Double-clad fibers

To maintain a good beam quality, the core of the active fiber has to be single mode. Pumping the single mode core with single mode laser diodes would provide ideal overlap but such laser diodes are limited in power. On the other hand, pumping a single clad fiber with a high power but multi-mode diode laser is extremely inefficient.

This problem was solved by the development of the 'double-clad' fiber design, which was first proposed by Snitzer *et al.*, in 1988 [29]. In this design, the high power multi-mode pump laser is coupled into a large inner cladding (ic) with refractive index lower than the core but higher than the outer cladding (oc) ($n_{core} > n_{ic} > n_{oc}$), so that the pump light is guided in the inner cladding by total internal reflection. When the pump light overlaps with the core, it is absorbed by the active dopants in the core and thus enables amplification of the seed light. Thus single mode beam quality can be maintained despite the use of high power multimode laser diodes as pump sources. Such fiber systems are said to be 'cladding pumped'. The schematic of a cladding pumped double-clad fiber amplifier is shown in Fig. 2.5.

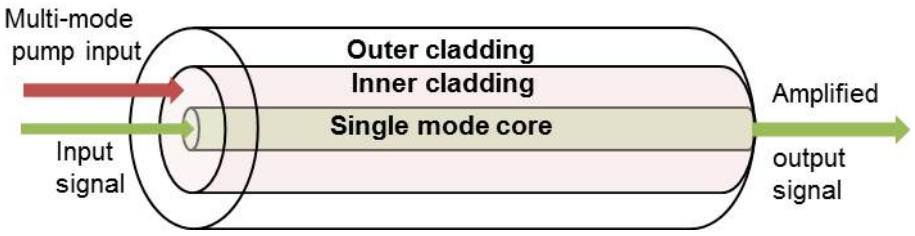

Figure 2.5: Schematic of a cladding pumped double-clad fiber amplifier.

The inherent advantage of a single-clad fiber, namely the excellent overlap of pump modes with the doped area, is lost in case of a double-clad fiber design. The simple centered circular core geometry shown in Fig. 2.5 is the easiest to fabricate and use. However, in such a structure, a large number of pump modes in the inner cladding have poor overlap with the core area, thus resulting in low efficiency of pump absorption in the core. This in turn reduces the gain and power efficiency of the active fiber.

Different inner cladding geometries have been proposed in order to increase the overlap of the pump modes with the core area [30, 31]. Some of the commonly used double-clad fiber designs with non-circular inner cladding geometry are shown in

Fig. 2.6. The octagonal inner cladding is one of the most common geometries used in commercially available double-clad fibers.

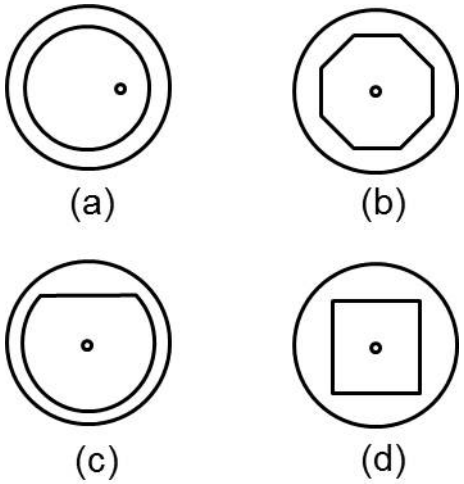

Figure 2.6: Different fiber inner cladding and core geometries used for increasing pump absorption: (a) offset core fiber, (b) octagonal inner cladding, (c) "D" shaped inner cladding, (d) square inner cladding.

2.3.2 Large mode-area fibers

The invention of cladding pumped schemes led to a rapid increase in the achievable output powers of fiber lasers. At such high powers nonlinear phenomena in the fibers become prominent. In order to minimize the effect of nonlinearities and to avoid the damage of the fiber, the core size has to be increased. This led to the introduction of large mode-area (LMA) fibers.

In general, increasing the mode area affects the single mode operation of the core and reduces the beam quality. There are two possible ways to maintain single mode operation while increasing the mode area: 1) the numerical aperture (NA) of the core should be kept small; 2) the guidance of the higher order modes must be kept weak. For conventional solid core fiber designs, a low NA core leads to a number of fabrication challenges and the weak guidance introduces significant losses in the fundamental mode. This limits the scalability of core area in conventional solid core fibers. These challenges were overcome by the development of a new class of fibers known by the term "Photonic crystal fibers", first coined by P. St. J. Russell in 1990s [32]. Light guidance in PCF is achieved either by total internal reflection or by photonic bandgap effect. PCFs have a closely packed arrangement of tiny holes

surrounding a solid or hollow core. By varying the dimensions of the hole arrangement, the numerical aperture can be tailored, thus enabling single mode operation over a wide wavelength range.

Combination of photonic crystal fibers and cladding pumped schemes led to the development of fiber lasers with extremely high output powers [33–36]. Despite careful fiber design, at such high powers thermal and nonlinear effects can cause significant damage to the fiber and the performance of the device. Some important nonlinear effects and noises in fiber devices are briefly described in the following subsection.

2.4 Noise and nonlinear effects

Apart from amplifying the input seed, an amplifier often produces excess unwanted components in the output known as noise. In an electrical amplifier the noise is often caused by thermal effects, whereas in an optical amplifier, the noise usually occurs in the form of spontaneous emission. Spontaneous emission is caused by the quantum effects in the gain medium and is typically non-directional. However, in a fiber-based gain medium, the large aspect ratio and wave guidance can cause a highly directional amplification resulting in amplified spontaneous emission (ASE). The most significant noise in optical amplifiers is due to ASE and it often limits the gain of the device. Apart from ASE, other quantum effects also limit the performance of optical amplifiers. One such effect is the excited state absorption (ESA), which results in loss of available atoms in excited energy levels due to absorption to higher energy levels, .

The long interaction lengths in fibers combined with the light confinement in a relatively small core area results in high optical intensities inside the core. Such high optical intensities lead to various χ^3 nonlinear effects in the fiber such as self-phase modulation, cross-phase modulation, four-wave mixing, Kerr-effect, Raman and Brillouin scattering. These nonlinear effects can serve as useful phenomena for broadening of light in applications such as supercontinuum generation. However, in most high power amplifier and laser applications, the nonlinearities are unwanted effects which limit the performance of the device or cause fiber damage.

Careful design of fibers is essential to neglect or tailor the noise and nonlinear effects. Besides the fiber designs, these effects are also highly dependent on the nature of the optical gain medium. For example, the spontaneous emission factor increases with the decrease in number of energy levels involved in the amplification process.

2.5 Ytterbium-doped gain media

Though the first Ytterbium-doped fiber laser was demonstrated as early as 1988 [11], Yb-doped fibers were not commonly used in the beginning. The main reason for this, was the popularity of Neodymium and Erbium doped fibers. Neodymium doped fibers exhibit a four-level behavior with highly efficient emission at 1060 nm wavelength for pumping at 800 nm. Erbium doped fibers have the advantage that their emission wavelength (1520 to 1600 nm) lies in the telecommunication wavelength region and they can be pumped at a number of wavelengths from 510 to 1480 nm. However, these systems have certain disadvantages, for example, excited state absorption in Erbium-doped fibers and limited emission bandwidth in Neodymium-doped fibers, which limits the gain and applications of such fibers. Therefore the attention turns to other rare-earth-doped fibers. A detailed study of various advantages of Ytterbium-doped fibers was presented by Paschotta *et al.*, in 1997 [37] and this served as a door to renewed interest in these fibers. The key characteristics of Ytterbium-doped gain medium which results in its numerous advantages are discussed in this subsection.

2.5.1 Electronic level structure of Yb^{3+} ions

The electronic structure of Yb^{3+} ions is shown in Fig. 2.7 [38], with only the two main energy levels involved in light amplification, the ground level manifold ($^2F_{7/2}$) and a higher excited manifold ($^2F_{5/2}$). These energy levels are split into sub-energy levels by the Stark effect and pump and laser transitions occur between various sub-energy levels as indicated in Fig. 2.7, by red and green arrows, respectively.

The main advantages of Ytterbium-doped gain media arise from the fact that only one excited state manifold is involved in the laser transition. The relatively small energy gap between the ground and excited-state results in extremely low quantum defects. Consequently high power efficiency is possible, and many detrimental effects such as thermal effects, quenching and excited state absorption are significantly reduced [39]. The low quantum defect also results in some disadvantages such as a pronounced quasi-3-level behavior.

Yb-doped fibers exhibit quasi-3-level or 4-level behaviors depending on the pump and seed wavelengths. For emission wavelengths less than 1080 nm, the lower laser transition state is located very close to the ground level (see Fig. 2.7) similar to a quasi-3-level system. There is significant population in this level at thermal equilibrium, which causes re-absorption losses [39] in the un-pumped gain medium and consequently, higher laser thresholds are required compared, for instance, to Nd-doped fibers [40]. Beyond 1080 nm, the laser transitions occur at energy levels

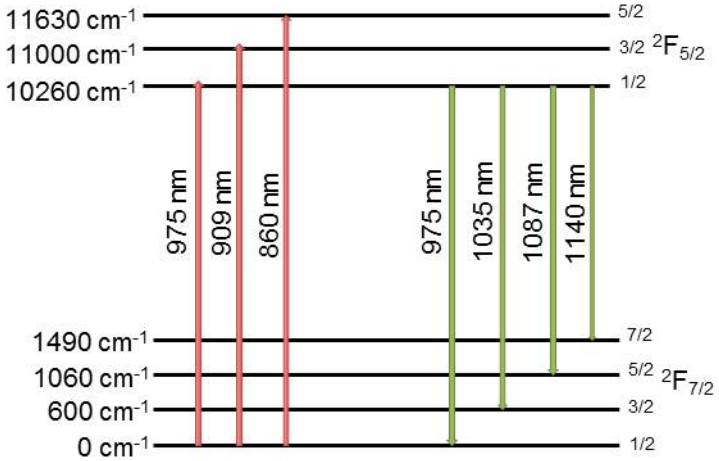

Figure 2.7: Yb^{3+} energy level structure, consisting of two manifolds, the ground manifold ($^2F_{7/2}$) (with four Stark levels), and higher excited manifold ($^2F_{5/2}$) (with three Stark levels). Approximate energies in wave-numbers above ground energy are indicated on the left side.

considerably higher than ground-level and hence the system exhibits a 4-level behavior. Due to the large energy gap between the ground level and lower laser level, population inversion is easily achieved and the laser threshold is reduced in this regime.

2.5.2 Spectroscopic data for Yb-doped fibers

The simple electronic structure of Yb-ions leads to highly pronounced absorption and emission cross-sections, which are also strongly dependent on the host medium of the Yb^{3+} ions. Germanosilicate glass is the most common host medium, which is typically the material used in Yb-doped fiber cores. The corresponding absorption and emission cross-sections, as presented in [37], are shown in Fig. 2.8.

The two peaks in the absorption cross-section provide the obvious choices for pump wavelengths. At 910 nm the absorption cross-section is broad but relatively low and strong pumping is required to achieve high gain. Nearly 97 % upper state population can be achieved [37] with strong pumping. However strong pumping can lead to significant ASE at 975 nm which in turn limits the maximum gain available for amplification at longer wavelengths. The high absorption cross-section at 975 nm results in very efficient pumping at this wavelength and the problem of ASE at 975 nm can also be avoided. However, since the absorption and emission cross-sections

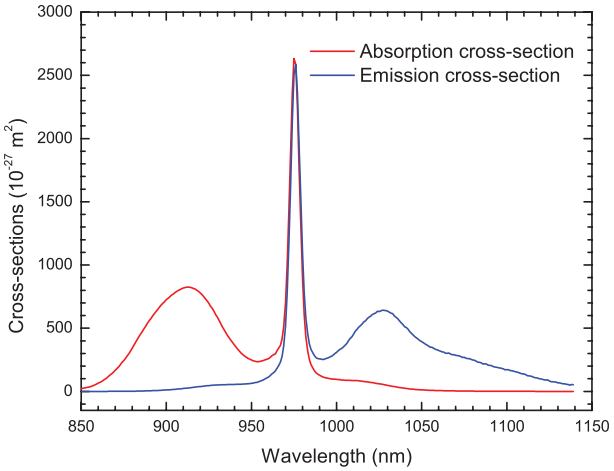

Figure 2.8: Absorption and emission cross-sections of Yb in germanosilicate glass [37].

are of almost equal magnitude at 975 nm, the maximum upper state population achievable is only 50 %. The narrow absorption peak also results in greater sensitivity to pump source parameters at this wavelength.

Gain can be achieved either at the narrow 975 nm emission peak or over a broader 1000 nm to 1100 nm range. The broad amplification bandwidth is highly suitable for ultra-short pulse amplifications. Due to a strong 3-level behavior at 975 nm amplification wavelength, the re-absorption loss in an un-pumped fiber is very high and the length of the fiber has to be carefully optimized. Though it was initially believed that the low quantum defect would avoid quenching effects, strong lifetime quenching was observed in Yb-doped fibers [41].

Despite the disadvantages such as re-absorption losses and pronounced ASE, Ytterbium-doped fibers offer many advantages such as high power efficiency, low thermal effects and high gain bandwidth. These advantages make them especially attractive for high power and ultra-short pulse propagation applications.

3 Modeling

Designing an efficient fiber device requires thorough understanding of its behavior under different conditions. Theoretical studies of such devices become inevitable in order to avoid time and cost consuming trial and error experimental methods. Extensive numerical and analytical models were developed in the early 1990s, to predict the behavior of rare-earth-doped fiber devices [42], in particular Erbium-doped fiber amplifiers [43–47]. The theoretical model for Ytterbium-doped fiber amplifier was first adapted from existing EDFA models [37], under certain simplifying assumptions. Several theoretical approaches have since been developed to model the effects of various parameters on the performance of Ytterbium-doped fiber devices in different configurations [48, 49].

The wavelength dependent behavior of Ytterbium-doped systems (as discussed in Section 2.5) results in a complicated interplay of pump, seed/laser and fiber parameters, which affect the gain profile significantly. Development of numerical methods required to accurately model such systems are typically complex and time consuming. The availability of proven simulation tools which can model such systems with considerable accuracy, would greatly benefit the research in this field.

The purpose of this chapter is to provide an overview of theoretical modeling of Ytterbium-doped fiber devices and to compare the performance of the RP-Fiber Power simulation model with a theoretical model. With this aim, a general two-level laser system is first described using rate equations and is then extended to a specific case of fiber waveguide structure where the interaction of light and matter is described using fiber properties. The light propagation equations and small signal gain co-efficient of a fiber device are derived and the gain spectrum specifically for Ytterbium-doped fibers is discussed in detail. Applying the general two-level system equations, theoretical modeling of Ytterbium-doped fiber lasers and amplifiers is explained. The RP-Fiber Power commercial simulation software is then introduced and the output power from the simulated fiber laser model is compared with the theoretical model.

3.1 Rate and propagation equations

Three-level systems can be described using a reduced two-level model [42], when the non-radiative relaxations to the meta-stable state are extremely rapid. At 975 nm pumping the Ytterbium-doped gain medium can be modeled using a simple two-level laser scheme shown in Fig. 3.1.

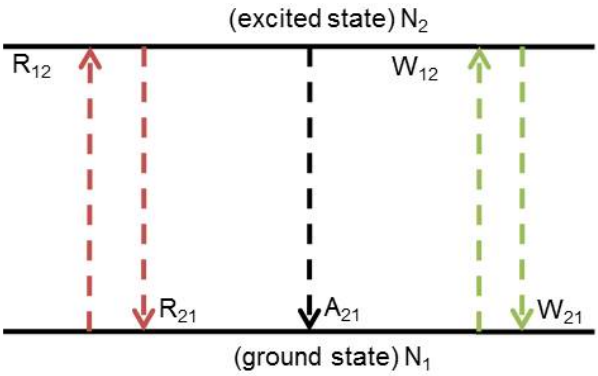

Figure 3.1: Energy level diagram for two-level system.

The relative population of Yb^{3+} ions in upper and lower energy levels are governed by the local rate equations:

$$\frac{dn_2}{dt} = (R_{12} + W_{12})n_1 - (R_{21} + W_{21} + A_{21})n_2 \tag{2}$$

$$\frac{dn_1}{dt} = -(R_{12} + W_{12})n_1 + (R_{21} + W_{21} + A_{21})n_2, \tag{3}$$

where n_1 and n_2 are the normalized populations in upper and lower energy levels ($n_i = N_i/N_t, i = 1, 2$), R_{12} and R_{21} are the pump excitation and de-excitation rates, W_{12} and W_{21} are the seed absorption and emission rates, respectively, and A_{21} denotes the spontaneous emission rate. By applying the energy conservation law, we arrive at

$$n_1 + n_2 = 1. \tag{4}$$

Under steady state conditions ($dn_i/dt = 0$),

$$n_1 = \frac{R_{21} + W_{21} + A_{21}}{R_{12} + R_{21} + W_{12} + W_{21} + A_{21}} \tag{5}$$

$$n_2 = \frac{R_{12} + W_{12}}{R_{12} + R_{21} + W_{12} + W_{21} + A_{21}}. \tag{6}$$

In a fiber waveguide, the pump and seed transition rates are governed by the absorption and emission cross-sections of the ions in the host medium and can be written as

$$R_{12} = \frac{\sigma_{ap} I_p}{h\nu_p}, \qquad R_{21} = \frac{\sigma_{ep} I_p}{h\nu_p}, \tag{7}$$

$$W_{12} = \frac{\sigma_{as} I_s}{h\nu_s}, \qquad W_{21} = \frac{\sigma_{es} I_s}{h\nu_s}, \tag{8}$$

where $\sigma_{ap}(\sigma_{ep})$ and $\sigma_{as}(\sigma_{es})$ are the pump and seed absorption(emission) cross-sections, respectively, and I_p and I_s are the corresponding intensities with transition frequencies ν_p and ν_s. The spontaneous emission rate is given by

$$A_{21} = \frac{1}{\tau}, \tag{9}$$

where τ is the life time of Yb^{3+} ions in the excited state. For a quasi-two-level fiber system defined by above equations, the variation of pump power along the fiber length is given by the propagation equation:

$$\frac{dP_p}{dz} = \Gamma_p N_t (\sigma_{ep} n_2 - \sigma_{ap} n_1) P_p(z), \tag{10}$$

where Γ_p is the pump overlap factor, defined as the ratio of pump core area over doped area (S_{pc}/S_d) and N_t is the total ion density. The propagation of seed along the fiber length can similarly be written as

$$\frac{dP_s}{dz} = \Gamma_s N_t(\sigma_{es} n_2 - \sigma_{as} n_1) P_s(z), \tag{11}$$

where

$$g(z) = \Gamma_s N_t(\sigma_{es} n_2 - \sigma_{as} n_1)), \tag{12}$$

is the small signal gain co-efficient. The seed overlap factor (Γ_s) is defined as the overlap of mode field area with doped area.

3.2 Gain spectrum

The distinct absorption and emission cross-sections of Ytterbium-doped gain media was discussed in section 2.5. In order to further illustrate the effects of pump and lasing wavelengths on the small signal gain of the device, the gain spectrum is plotted for different wavelengths. From Eq. 12, the small signal gain at any wavelength can be calculated from the absorption and emission co-efficients at that wavelength and the relative population of Yb^{3+} ions in the two energy levels. The relative inversion (RI) in the two-level system can be written as

$$RI = n_2 - n_1. \tag{13}$$

Assuming a total Yb^{3+} ion concentration (N_t) of $1e^{26}$ m^{-3} and an ideal case where the light propagates only in the doped area (*i.e.*, Γ_s=1), Eq. 12 can be expressed as

$$g(z) = \frac{1e^{26} * (\sigma_{el}(1 + RI) - \sigma_{al}(1 - RI))}{2}, \tag{14}$$

for any wavelength l. The gain spectrum at different wavelengths (Eq. 14) is plotted in Fig. 3.2 for a Ytterbium-doped fiber with absorption and emission cross-sections as presented in [37], for varying levels of relative inversion, where RI=1 and RI=-1

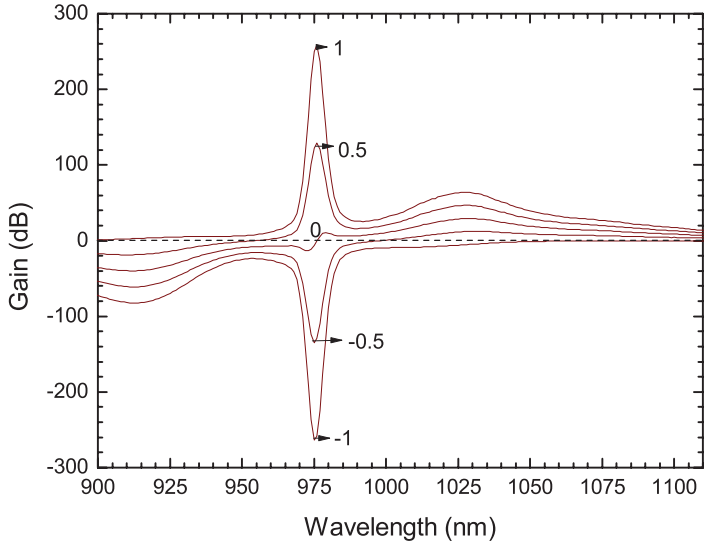

Figure 3.2: Gain spectrum at different wavelengths for varying levels of relative inversion.

denote complete and zero population inversion, respectively.

The plot for RI=0 shows the gain spectrum at 50 % population inversion, which is achieved in case of pumping at 975 nm wavelength due to equal absorption and emission cross-sections at this wavelength. For this level of population inversion, the maximum gain occurs close to 1035 nm. Higher levels of population inversion ($0<RI<1$) can be achieved by pumping at shorter wavelengths, where it is seen that the maximum gain occurs at 975 nm. This limits the gain available for amplification at higher wavelengths due to strong ASE at 975 nm. The negative gains observed in case of low levels of population inversion ($0>RI>$-1) indicate that there is strong re-absorption at all wavelengths in an un-pumped gain medium. The length of Ytterbium-doped fiber has to be carefully tailored to avoid this re-absorption.

3.3 Fiber laser theory

A linear cavity Ytterbium-doped fiber laser can be modeled from the two-level system equations described in section 3.1, by applying the boundary conditions for resonator cavity and by setting the net round-trip gain to unity. The schematic of a counter-pumped linear cavity fiber laser is shown in Fig. 3.3.

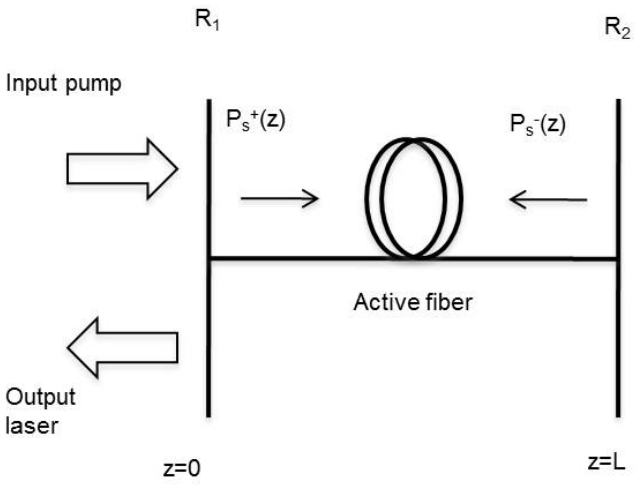

Figure 3.3: Schematic of counter-pumped linear cavity fiber laser.

The boundary conditions for forward(P_s^+) and backward(P_s^-) propagating laser, respectively, are

$$P_s^+(0) = R_1 P_s^-(0), \tag{15}$$

$$P_s^-(L) = R_2 P_s^+(L) \tag{16}$$

and

$$P_s^-(z) P_s^+(z) = constant \tag{17}$$

where R_1 and R_2 are the reflectivities of the resonator cavity. For the counter-propagating scheme shown in Fig. 3.3, the gain is obtained by integrating the gain coefficient $g(z)$ given in Eq. (12) over the length of the fiber as

$$\begin{aligned} G = & \int_0^L g(z)dz \\ = & \Gamma_s N_t \int_0^L [\sigma_{es} n_2 - \sigma_{as} n_1] dz. \end{aligned} \tag{18}$$

The stationary condition for a linear cavity fiber laser is given by

$$R_1 R_2 exp(2G) = 1. \tag{19}$$

By substituting the propagation equations (10) and (11) in Eq. (18) and by applying the stationary condition as shown in [17], the gain is obtained as

$$\begin{aligned} G_p = & \quad \ln[P_p(L)/P_p(0)] \\ = & \quad \frac{\Gamma_p \sigma_p}{2\Gamma_s \sigma_s} \ln(\frac{1}{R_1 R_2}) - \frac{\sigma_{es}\sigma_{ap} - \sigma_{ep}\sigma_{as}}{\sigma_s} \Gamma_p N_t L. \end{aligned} \tag{20}$$

From the above equations, the output power of the laser can be obtained as

$$\begin{aligned} P_{out} = & \quad (1 - R_1) P_s^-(0) \\ = & \quad \frac{\lambda_p}{\lambda_s} . \frac{(1 - R_1) P_p^{sat}}{1 - R_1 - \sqrt{R_1 R_2} + \sqrt{\frac{R_1}{R_2}}} \\ & \times [\frac{P_p(0)}{P_p^{sat}} (1 - exp(G_p)) - G_p - \Gamma_p N_t \sigma_{ap} L]. \end{aligned} \tag{21}$$

When P_{out}=0, Eq. (21) gives the laser threshold power

$$P_{th} = P_p^{sat} \times \frac{G_p + \Gamma_p N_t \sigma_{ap} L}{1 + exp(G_p)}. \tag{22}$$

3.4 Fiber amplifier theory

A simplified analytical solution for EDFA using the two-level model described in section 3.1 was first proposed by Saleh *et al.* in 1990 [43]. This model requires only the knowledge of two easily measurable fiber parameters namely the attenuation coefficient (σ) and the intrinsic saturation power (P_{sat}) corresponding to each wavelength propagating through the fiber. It was later argued [37, 42] that a Ytterbium-doped fiber amplifier operating at shorter emission wavelengths (<1080 nm) can be described using this reduced two-level model.

Certain simplifying assumptions have to be used in these models: 1) The power extracted by ASE must be negligible, which is valid for a fiber amplifier with input seed power significantly higher than equivalent ASE noise in the channel. 2) The field and dopant distributions must be homogeneous, which is typically the case for single mode doped fiber cores. 3) Excited state absorption must be absent, which is true for Ytterbium-doped fibers. Under such simplifying assumptions, the upper-level steady state population can be obtained from Eqs. (6)-(8) as:

$$n_2 = \frac{\sigma_{ap}\sigma_s P_s^{sat} P_p + \sigma_{as}\sigma_p P_p^{sat}(P_s)}{\sigma_p\sigma_s P_p P_s^{sat} + \sigma_p\sigma_s P_p^{sat}(P_s) + \sigma_p\sigma_s P_p^{sat} P_s^{sat}}. \tag{23}$$

The pump and seed saturation powers P_p^{sat} and P_s^{sat} are

$$P_p^{sat} = \frac{h\nu_p A}{\Gamma_p \sigma_p \tau} \tag{24}$$

$$P_s^{sat} = \frac{h\nu_s A}{\Gamma_s \sigma_s \tau}, \tag{25}$$

where A is the effective core area, $\sigma_p(=\sigma_{ep}+\sigma_{ap})$ and $\sigma_s(=\sigma_{es}+\sigma_{as})$ are the pump and seed attenuation coefficients, respectively. Substituting Eq. (23) in the pump and seed propagation equations (10) and (11) and by integrating them over the length of the fiber L, the coupled equations for the output pump and seed powers independent of propagation directions can be obtained as:

$$P_p^{out} = P_p^{in} exp[-\sigma_p L + \frac{P_p^{in} - P_p^{out} + P_s^{in} - P_s^{out}}{P_p^{sat}}] \tag{26}$$

$$P_s^{out} = P_s^{in} exp[-\sigma_s L + \frac{P_s^{in} - P_s^{out} + P_p^{in} - P_p^{out}}{P_s^{sat}}]. \tag{27}$$

Standard root-finding techniques can be applied to solve the coupled equations [42]. In conditions where the ASE cannot be neglected, the propagation of ASE must be calculated separately for number of wavelengths and for each propagation direction [37].

3.5 RP-Fiber Power simulation software

The models described in sections 3.4 and 3.3 are for the continuous wave operation regime. For propagation of a pulsed light through the fiber, nonlinear effects and dispersion such as group velocity dispersion (GVD) have to be taken into account. Iterative numerical solutions are essential in order to obtain self-consistent solutions for such systems, and the computation time and complexity are greatly increased. Multi-level fiber systems and advanced fiber designs further increase the difficulty in modeling. With increasing popularity of fiber devices, commercial software tools are beginning to emerge in order to facilitate the understanding and design of such devices. RP-Fiber Power is one such software for simulating light propagation in optical fibers. Some key features of the software are presented in this section.

RP-Fiber Power enables the modeling of both passive as well as active fiber devices from fiber specifications and spectroscopic data. The software includes a mode-solver feature to analyze the distribution of modes in the fiber. Arbitrary optical channels for different pump and seed/laser light can be defined by specifying the input powers, wavelength, radial function for intensity profile, losses and propagation direction (backward or forward). ASE channels can also be defined in a similar manner where the input powers are spontaneous emission values calculated automatically by the software from fiber cross-section data. Reflectivities for each of the optical channels can be independently defined. Radial dependence of doping profile can be accurately modeled in the software by defining the doped region as individual radial sections. Even in fibers with uniform doping profile, this functionality can be used to refine the calculations by taking into account the radial

variation of optical intensities in the core.

Devices can be defined using a graphical form based input or a script editor. Multistage devices like master oscillator power amplifier (MOPA), can be designed with flexibility. Numerical solutions of rate equations and propagation equations are used to model continuous wave and dynamic systems. Ultra-short pulse propagation in the fiber, which is modeled by solving Nonlinear Schrödinger Equation (NLSE), can also be studied. Evolution of excited state population, variation of powers along the fiber length, growth of noise, ASE and other nonlinearities, and the temporal evolution of pulse parameters can be examined using graphical outputs.

3.6 Comparison of simulation and theoretical models

In order to verify the performance of the simulation software, a double-clad fiber laser similar to the one used in section 3.3 is simulated and the laser output powers for various pump powers is compared to the outputs calculated from Eq. (21) of the theoretical laser model. A Ytterbium-doped double-clad fiber with absorption and emission spectra as presented in [37] and fluorescence life time 0f 0.9 ms is considered to be the active fiber. The core and inner-cladding diameters are assumed to be 20 μm and 125 μm, respectively. The numerical aperture of core is assumed to be 0.1 and the cladding absorption at pump wavelength is assumed to be 12 dB/m. The fiber length is assumed to be 2 m, and the reflectivities R_1 and R_2 are assumed to be 1 % and 100 %, respectively.

For the purpose of modeling, the pump beam is assumed to have a top-hat intensity profile in the inner-cladding. A 976 nm pump wavelength is used and the lasing wavelength is assumed to be 1040 nm. For the counter propagating scheme used, the backward light gives the laser output. The laser output powers from the simulation and theoretical models are plotted in Fig. 3.4.

The slope efficiency of both theoretical and simulation output was estimated to be 92.8 %. The laser threshold power was calculated theoretically using Eq. 22 to be 584 mW and the laser threshold estimated from simulation output was 590 mW. This give $\sim$ 99 % agreement between the simulation and theoretical models.

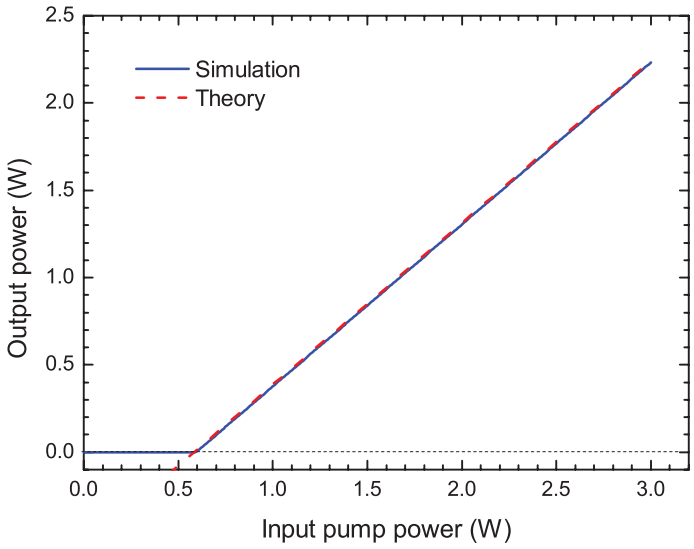

Figure 3.4: Theory versus simulation.

The simulation model can be used to study propagation of powers along the fiber length, distribution of upper-state population, and effect of fiber length in the form of graphical outputs. In Fig. 3.5 (a) and (b), the variation of optical powers for different light along the length of a fiber with zero end reflectivities and with 1 % (left) and 100 % (right) end reflectivities, respectively, are shown. In case of zero reflectivities, the pump power decreases almost linearly along the length of the fiber. The initial excitation level achieved for a 976 nm pump input of 3 mW is close to 40 % and the excitation remains almost constant upto 1 m of the fiber. When the reflectivities are included, lasing occurs and the overall excitation level achieved for the input pump power is slightly less than 20 %.

The effect of the total length of fiber used can be understood from Fig. 3.6. For the given fiber specifications, it is seen that the input pump power of 3 mW gets completely absorbed in 2 meters of length. However, the maximum laser output is obtained for a fiber length of approximately 1.4 m and for longer fiber lengths, re-absorption of the laser is seen in Fig. 3.6. This graphical output can be used to obtain information about the ideal length of fiber to be used in the setup.

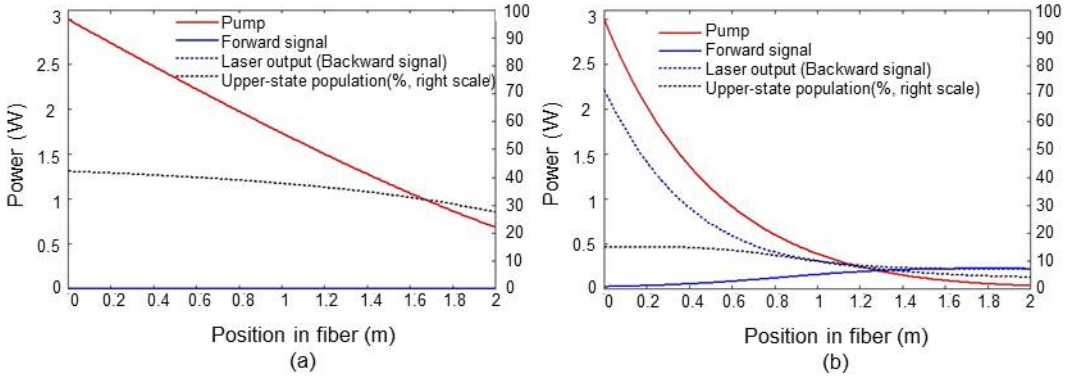

Figure 3.5: Variation of powers along fiber length for (a) zero reflectivities, (b) 1 % and 100 % reflectivities.

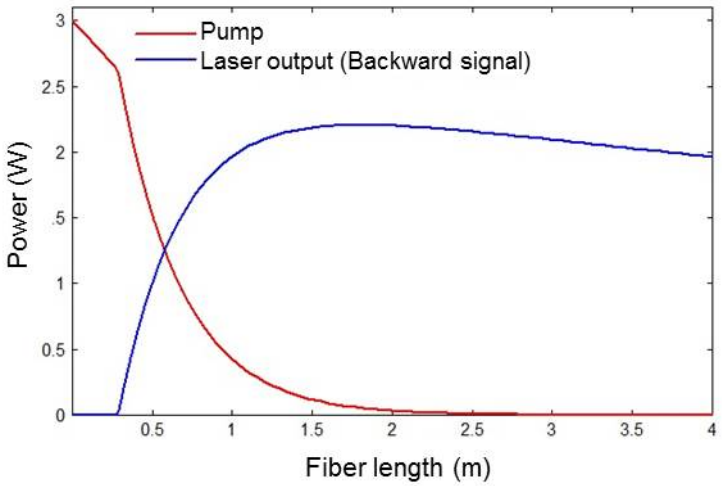

Figure 3.6: Effect of fiber length.

4 Experiments

The main objective of this experimental work is to realize a low power fiber amplifier operating in the continuous wave regime using Ytterbium-doped fibers. As discussed in section 2, amplified spontaneous emission is the most dominant noise factor in Ytterbium-doped fibers. The presence of even small reflectivities of the order of few percentage can cause onset of lasing in ASE spectrum. This can seriously affect the performance of a fiber amplifier. In order to study the self-lasing in the chosen active fibers, a simple fiber laser with a Fabry-Perot cavity is first designed and then an amplifier for low power continuous wave light amplification is designed The experimental setups for the fiber laser and amplifier and the measurement results are presented in detail in this section.

4.1 Active fibers

Two different active fibers, Yb1200-20/125DC and Yb600-20/125DC, have been used for the experiments described in this chapter. Both fibers have a large core diameter of 20 μm with a small numerical aperture, enabling excellent beam quality. The inner cladding is octagonal shaped in order to optimize pump absorption, with a flat-to-flat diameter or 125 μm. The Yb1200 fiber has a high doping concentration resulting in a high cladding absorption of 6.8 dB/m, thus making it suitable for short length (less than 2 m) applications. In contrast, the Yb600 fiber has a lower doping concentration and correspondingly a cladding absorption of around 3.2 dB/m thus making it ideal for low power applications. The specifications of the two active fibers are summarized in Table 4.1.

Absorption and emission cross-sections for the Yb1200-20/125DC fiber given by the manufacturer are plotted in Fig. 4.1. They are compared to the cross-sections of a Yb-doped germanosilicate glass fiber as presented by Paschotta *et al.* in [37]. Though the general characteristics are the same, slight differences can be observed in the cross-section values. The absorption and emission cross-sections provided by Liekki have a slightly lower value at 975 nm, however the emission cross-section is significantly higher in the 1000 to 1150 wavelength range, compared to typical values.

4.2 Pump sources calibration

The 975 wavelength region is chosen for pumping the active fibers. In this region, the cross-section is very narrow and hence the system is highly sensitive to the actual pump wavelength. Thus characterization of the pump source is essential.

Table 4.1: Active fibers' specifications.

Parameter	**Yb600-20/125DC**	**Yb1200-20/125DC**
Core diameter (μm)	20±2	20±2
Core NA	0.08±0.01	0.08±0.01
Cladding shape	Octagonal	Octagonal
Cladding diameter, flat to flat (μm)	125±2	125±2
Cladding NA	0.46	0.46
Cladding absorption at 920 nm (dB/m)	3.4±0.7	6.8±1.7

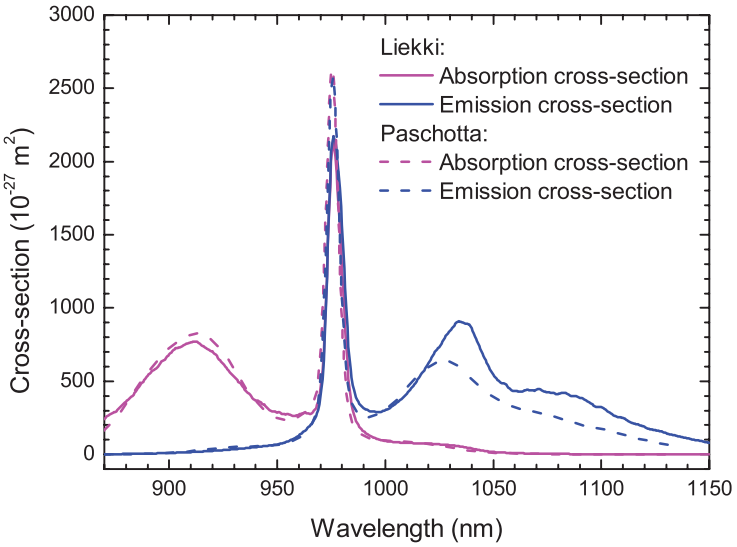

Figure 4.1: Absorption and emission cross-sections of Yb1200-20/125DC fiber given by Liekki versus the cross-section values for Yb-doped germanosilicate fibers as presented in [37].

Two different pump sources are used in the experiments. One of the pump sources is a diode laser (UM2800/50/15) from 'Unique-mode laser technology', referred to as UMLD in the following text. The diode laser has a high brightness, multi-mode continuous wave output which is coupled to a multi-mode fiber of 50 μm core with 0.15 numerical aperture and 125 μm cladding. The maximum output power was measured to be 2.6 W at 25^o C operating temperature. Output powers

and emission spectra of the pump source are measured at selected current inputs and the values are plotted in Fig. 4.2 (a) and (b), respectively. The emission spectrum shows slight dependence on driving current, shifting from 972.5 nm at low current inputs to 973 nm at higher currents. The full-width half-maximum (FWHM) is less than 5 nm at all current inputs.

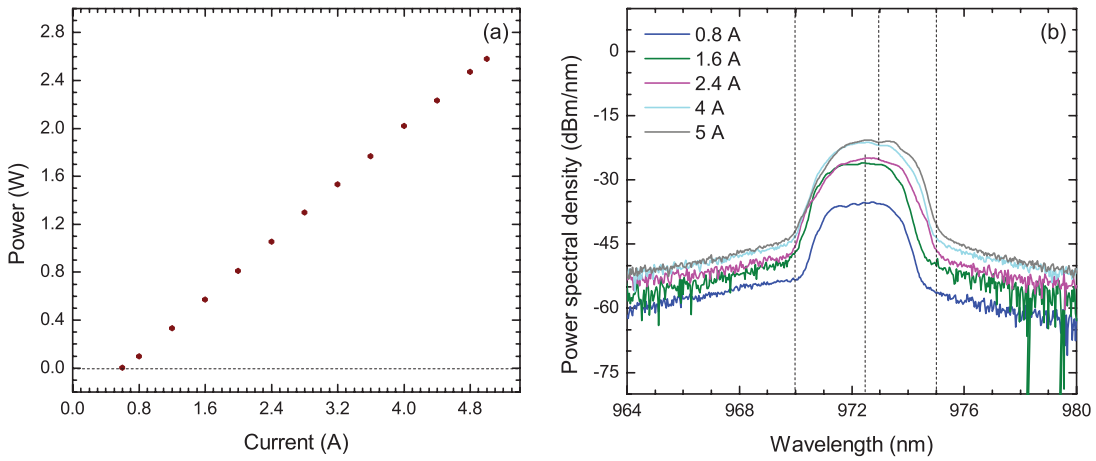

Figure 4.2: Calibration of UM2800/50/15 diode laser (a) Current versus power curve and (b) Spectrum at different currents.

The other pump source is a diode laser (BLD-98-0.5.25W-06-F-10-M) from 'Laser Components', referred to as BLD in the following text. The diode laser can provide continuous wave output up to 25 W at an operating temperature of 25^o C, however for this thesis work, only powers upto 7 W are used. The laser output is fiber coupled to a 105 μm core multi-mode fiber with a numerical aperture of 0.22. Output powers are measured by varying the driving current and the emission spectra are observed at selected current inputs. The values are plotted in Fig. 4.3 (a) and (b), respectively. The laser spectrum has a narrow bandwidth (FWHM less than 3 nm) and a central wavelength of 975.7 nm at all powers.

4.3 Fiber laser design

A Yb-doped double-clad fiber laser in counter propagating pump scheme, similar to the theoretical model described in section 3.3, is experimentally realized using a 1.75 m long Yb-1200-20/125DC fiber (specifications: see Table 4.1). The experimental setup is shown in Fig. 4.4.

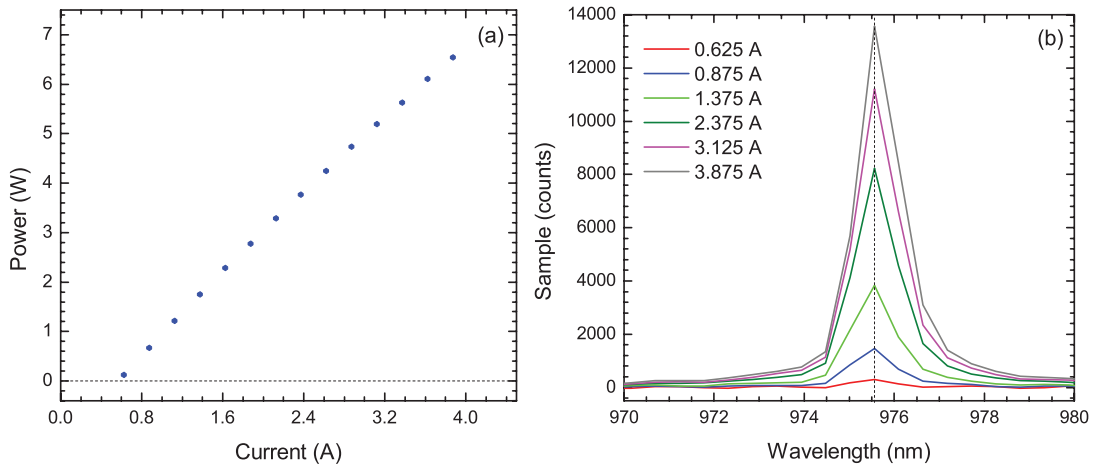

Figure 4.3: Calibration of BLD-98-0.5.25W-06-F-10-M diode laser (a) Current versus power curve and (b) Spectrum at different currents.

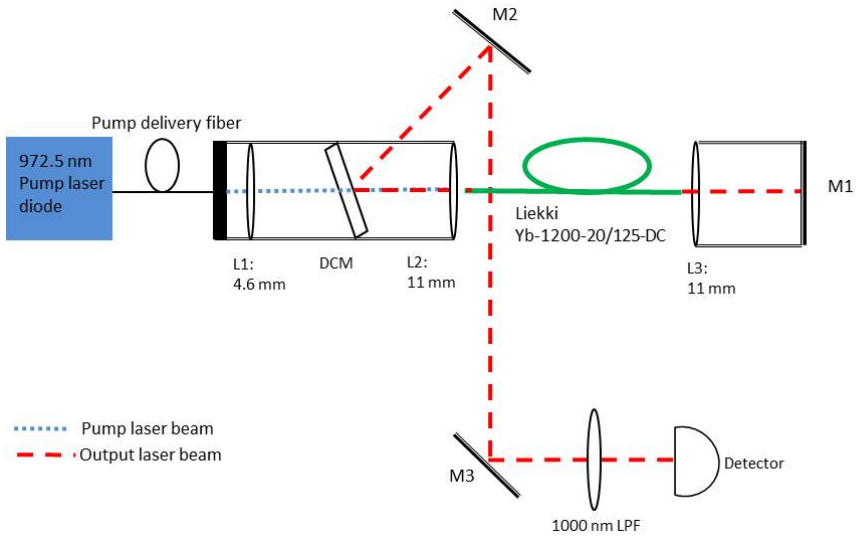

Figure 4.4: Fiber laser experimental setup.

The laser resonator cavity is formed by end reflections from the fiber facet on one end and a high reflection metallic mirror (M1) on the other end, referred to as left and right ends, respectively, in the following text. The fiber facet at the left end is nearly perpendicularly cleaved and the end reflection is estimated to be below Fresnel reflection value (<4 %). The fiber ends are mounted on xyz-translation stages for precise alignment. The UMLD laser source is used to pump the active fiber. The pump light emitted from the multi-mode fiber is collimated by a lens (L1) of 4.6 mm focal length.

To separate the emitted laser light from the pump light in the counter-propagating scheme, a DCM of high transmissivity (T>95 %) at wavelengths less than 1000 nm and high reflectivity (R>99 %) in the 1000 to 1200 nm wavelength range is placed between lenses L1 and L2. Pump light is focused into the inner cladding using a 11 mm lens (L2), which also serves to collimate the output light from the active fiber.

At the right end, laser and residual pump light output from the fiber is collimated by a 11 mm lens (L3) and reflected back into the fiber by a wavelength independent metallic mirror (M1) with high reflectivity R>99 %. At the left end, laser output (bacward propagating) is reflected by the DCM at 20^o angle and is aligned parallel to the optical table using metallic mirrors M2 and M3. A 1000 nm long pass filter (LPF) with 84 % transmissivity above 1000 nm, is used to block any residual pump light reaching the power meter.

Measurements

The laser output power is optimized by tuning the pump coupling stage and the mirror reflection arrangement on the right side. The position and coiling of the fiber are crucial and can significantly influence the performance of the laser up to 20 % at higher powers. Fiber coiling is optimized to get the best possible output powers within the scope of the setup and then kept undisturbed at this position for the duration of the measurements. The pump powers are varied from 0 to 3 W and the laser output powers and spectra are measured.

Pump coupling

In order to estimate correctly the actual pump powers coupled into the active fiber, independent measurements were performed without disturbing the pump alignment after the laser measurements were recorded. A cut-back approach was used and unabsorbed pump powers were estimated for different input pump powers, at different fiber lengths between 16 to 50 cm. The fiber was kept straight during these measurements. As example, the measured data for two different input powers are plotted in Fig. 4.5.

In the unsaturated regime, the remaining light power P_{out} at the end of an optical fiber can be described according to Beer's law as

$$P_{out} = P_{in} exp(-\alpha L) \tag{28}$$

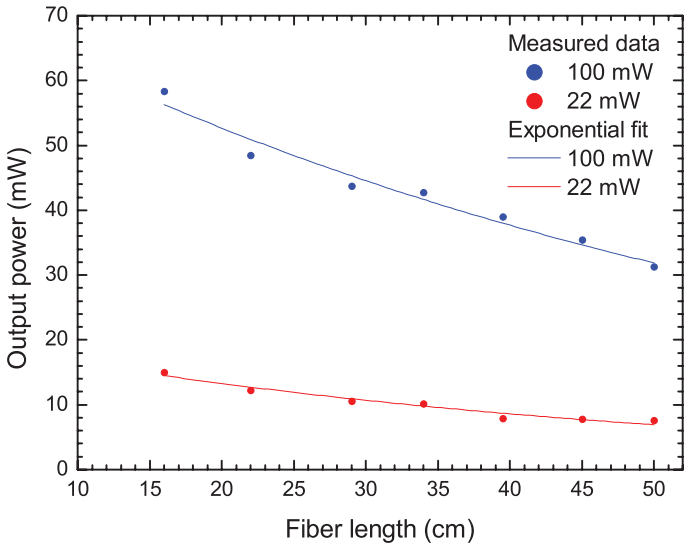

Figure 4.5: Unabsorbed pump powers measured at different lengths for two input powers.

where P_{in} is the light power at the fiber input, α is the fiber absorption coefficient and L is the length of the fiber. Operating at pump powers where ASE can be neglected, the measured light at the fiber output can be assumed to have the same spectral content as at the input, i.e. the measured output power is equivalent to the unabsorbed pump power as given by Eq. (22). From fitting Eq. (22) to the measured data, we can thus extract the coupled input powers. The results are summarized in Table 4.2.

The ratio between P_{in} and the measured power before the fiber yields the coupling efficiency. A weighted average of the measurements yields a coupling efficiency of 71.1±0.9%.

The average absorption co-efficient is calculated to be 6.89±0.17 dB/m. This value is about a factor of two smaller than the specified fiber absorption at 973 nm. The reason for this can be a shift of pump central wavelength towards 972 nm at these low powers (see Fig. 4.2), where the absorption cross-section of Liekki fiber is about 35 % lower than at 973 nm. More accurate absorption measurements require using longer fiber lengths, where the absorption is not so sensitive on the wavelength.

Table 4.2: Pump coupling estimation.

Power before fiber (mW)	**P_{in} from fit (mW)**	**Fit error in P_{in} (± mW)**	**Pump coupling (%)**	**Error in pump coupling (± %)**
100	73.6	3.22	73.82	3.23
90	62.87	1.71	70.17	1.91
78	54.93	1.99	70.06	2.55
66	47.27	1.45	71.19	2.19
55	40.16	1.05	72.89	1.9
44	30.25	1.08	68.90	2.46
32	24.67	1.24	77.59	3.89
22	20.51	1.26	94.94	5.82

Measurement results

The measured data is corrected for the transmission efficiency of 1000 nm LPF (84 %) and losses along the output path (5 %). The corrected measurement data is plotted with respect to the coupled pump powers along with pump coupling error bars in Fig. 4.6. A linear fit to the corrected measurement data yields a slope efficiency of 90 % and a lasing threshold of 815 mW.

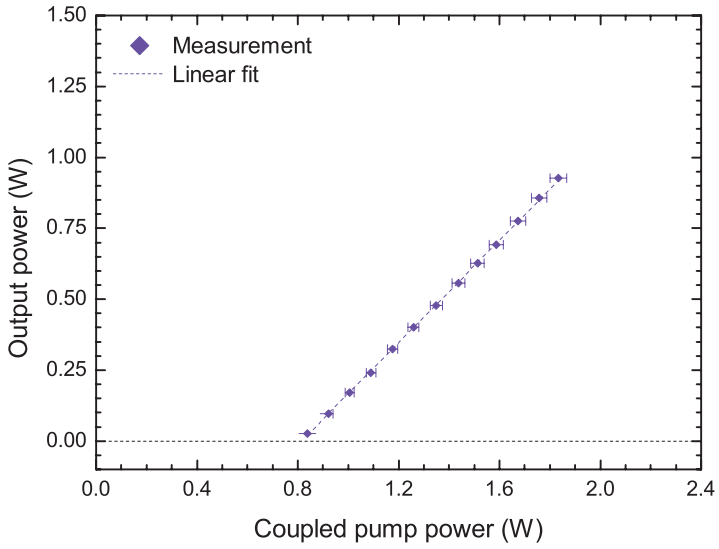

Figure 4.6: Fiber laser: Corrected measurement data.

For selected pump powers, the measured laser output spectra are shown in Fig. 4.7. At coupled pump powers below 0.8 W, a broad spectrum of ASE is observed in the 1030 to 1050 nm wavelength region. When the lasing threshold is reached, the spectrum narrows down to a wavelength range of about 4 nm around 1040 nm. The bandwidth and central wavelength show slight changes with increase in pump powers. For high input pump powers above 1.5 W, the spectrum stabilizes at a central wavelength of 1040 nm with a full width half maximum (FWHM) around 6 nm.

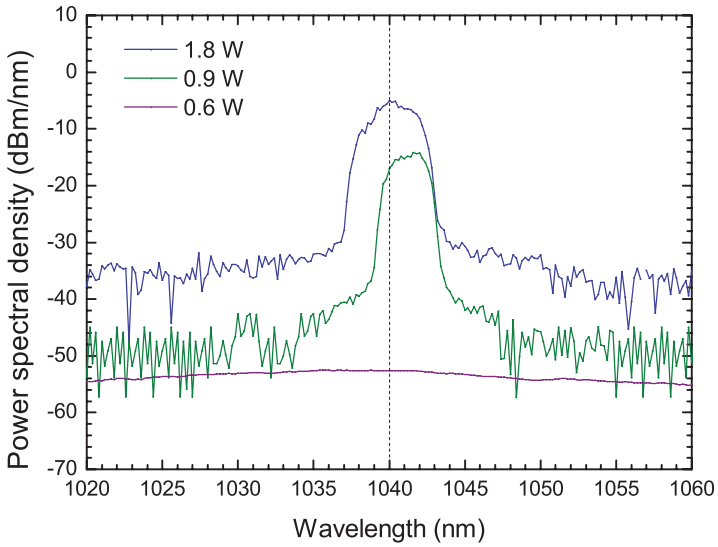

Figure 4.7: Laser output spectrum for different coupled pump powers.

4.4 Fiber amplifier design

A low power fiber amplifier operating in the continuous wave region is designed in a counter-propagating pump scheme. The Ytterbium-doped double-clad fiber used as active fiber is Yb600-20/125DC. The experimental setup is shown in Fig. 4.8.

A diode laser (Picopower-LD-1064-SF) from 'Alphalas' is used as the seed source. The diode laser provides a single-mode output at 1064 nm wavelength and can be operated in the continuous wave regime upto powers of 10 mW. The source is fiber coupled to a polarization maintaining fiber (PM980) with 6.6 μm mode field diameter and 0.12 numerical aperture.

Seed light from the PM fiber is collimated using a 11 mm lens (L1) and passed through a Faraday Isolator. A dichroic mirror (DCM1) with 99 % reflectivity at seed wavelength is used to reflect the output from the isolator at 45^o angle and another

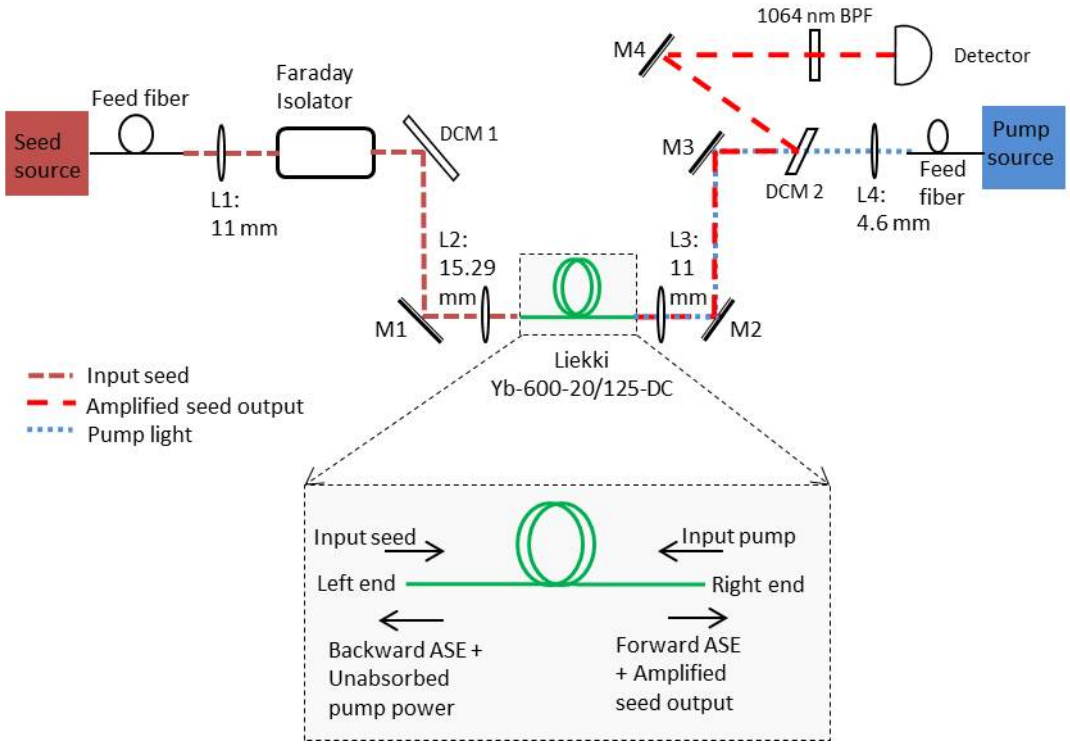

Figure 4.8: Fiber amplifier experimental setup, with inset showing direction and naming of different light beams propagating in the fiber.

metallic mirror with very high reflectivity (R>99 %) at all wavelengths, is used to align the beam parallel to the optical table. The seed light is then focused into the core of the active fiber using a 15.29 mm lens (L2). A 3 m long active fiber is used and the fiber is coiled with a 15 cm diameter. The left and right fiber end facets are cleaved with 1^o and 3.5^o angles, respectively and the fiber tips are mounted on xyz-translational stages to allow precise coupling of seed and pump light. A free-space optical setup is used for seed and pump coupling as opposed to an all fiber setup.

Pump light from the BLD source (see section 4.2) feed fiber is collimated using a 4.6 mm lens (L4) and passed through a dichroic mirror (DCM2) of high transmissivity (T>95 %) at wavelengths less than 1000 nm and high reflectivity (R>99 %) in the 1000 to 1200 nm wavelength range. Two metallic mirrors (M2 and M3) are used to align the collimated pump beam parallel to the optical table and a 11 mm lens (L3) is used to focus it into the right end of the active fiber. L3 also serves to collimate the output light from the active fiber which then travels the same path as pump beam and is reflected by DCM2 at 20^o. A metallic mirror (M4) is used to align the reflected light parallel to the optical table and the amplified seed output

is measured at the detector after a 1064 nm BPF. All metallic mirrors used in the setup have high wavelength independent reflectivity (R>99 %).

Measurements

In order to attain good amplification, it is essential to minimize the end reflections from the fiber facets. This can be achieved by various techniques such as use of index matching liquids in case of fiber to fiber coupling, or by angle cleaving the fiber facets [3]. In this experimental setup the fiber facets are cleaved with small angles of (approximately 1^o and 3.5^o at the left and right ends, respectively) to reduce end reflections. The effects of these cleave angles are studied by measuring the outputs from left and right fiber ends (referred to as the backward and forward light, respectively) for different pump input powers, without any seed coupling.

At the left fiber end, the backward light is measured just behind L3. At the right fiber end, the forward light is measured after reflection by DCM2 and M4 (see Fig. 4.8). A 1000 nm LPF is used before the detector during measurements to block any unabsorbed and back reflected pump light from the left and right ends, respectively. The spectrum is also observed during these measurements. Pump coupling is estimated to be 75±2 % as typically observed during independent cut-back measurements and all measurements in the amplifier setup are corrected correspondingly. The output powers and spectra of light measured from the fiber ends are plotted in Figs. 4.9 and 4.10, respectively.

For coupled pump powers above 1 W, linear increase in output powers were observed in both forward and backward light, which were found to have strong and narrow spectra in the 1030 to 1040 nm wavelength region for these pump powers . This indicates that the light measured at left and right fiber ends are the noise due to ASE propagating in the backward and forward directions, respectively. Also, the finite reflectivities from fiber end facets cause parasitic lasing of ASE (noise), for coupled pump powers above 1 W.

The forward and backward light measurements are fitted with linear functions to estimate the slope efficiencies and lasing thresholds (see Fig. 4.9). Both outputs have a lasing threshold of about 1 W but the lasing slope efficiency with respect to coupled pump power is much higher in the forward propagating ASE (76.7 %) compared to the backward ASE (6.2 %). This indicates that the reflectivity at right end facet, from which the backward ASE is reflected, is much lower than the reflectivity at the left end facet from which the forward ASE is reflected ($R_2<R_1$).

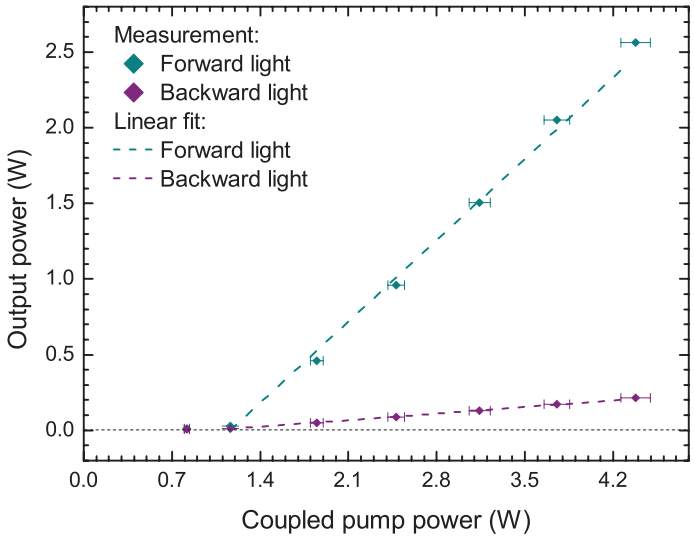

Figure 4.9: Output powers measured at left and right fiber ends in amplifier setup for zero seed input.

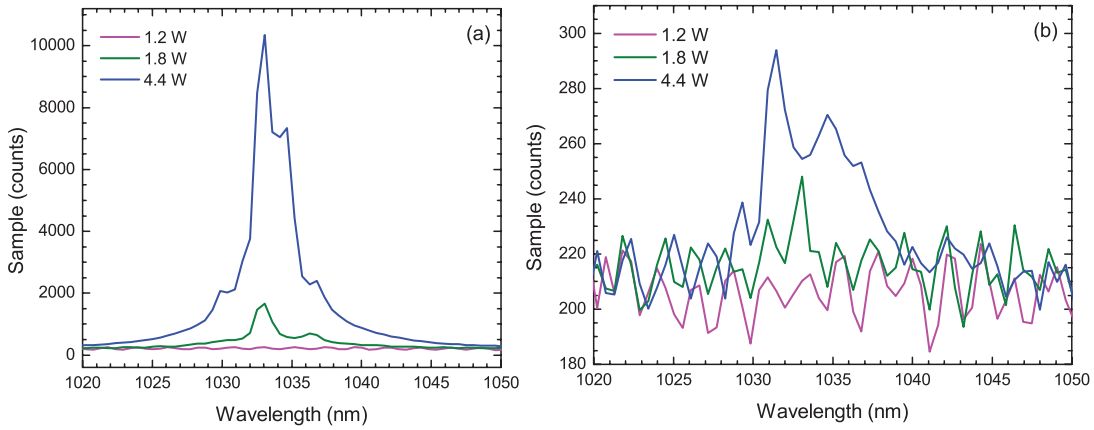

Figure 4.10: Spectrum at (a) left and (b) right fiber ends for different coupled pump powers.

Thus we conclude that a cleave angle of 3.5^o has lowered the reflectivity significantly at the right fiber facet but the reflectivity from left fiber facet (with 1^o cleave angle) is high enough to produce strong lasing at ASE wavelength in the forward direction when no seed is coupled.

The setup is then used to study continuous wave amplification by coupling a 6.7 mW seed input to the left fiber end. The amplified seed output reflected by DCM2 and M4, is measured for different pump input powers. A 1064 nm BPF is used to

measure the amplified seed without any contribution from the background noise. Measured output powers are corrected for the filter transmission efficiency and are plotted in Fig. 4.11, against coupled pump powers.

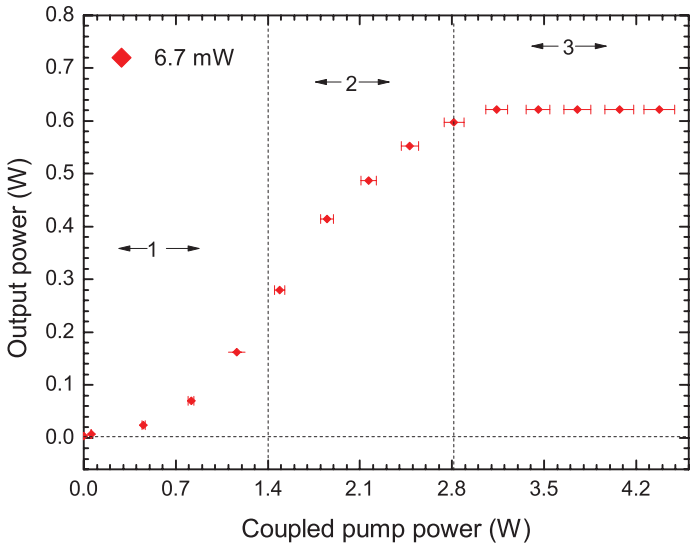

Figure 4.11: Amplified seed measurements for 6.7 mW seed input power.

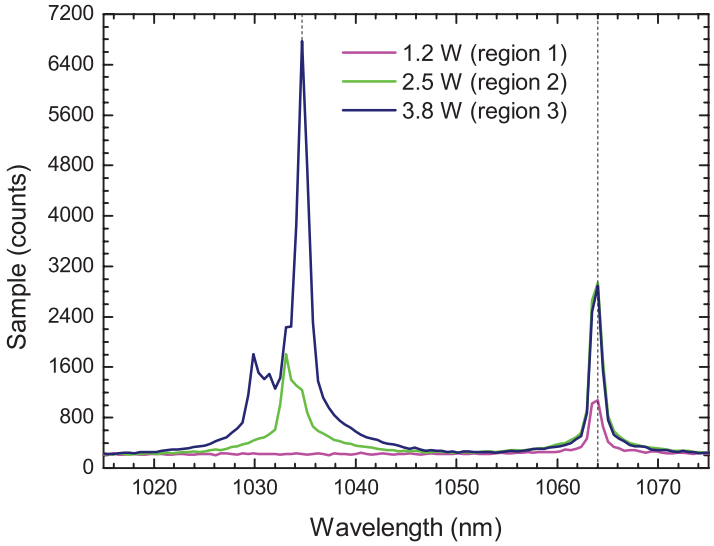

Figure 4.12: Output spectra for selected coupled pump powers.

In the amplified seed measurements, three distinct regions are observed as indicated in Fig. 4.11: In region 1, at coupled pump powers less than 1.4 W, am-

plification is exponential, in region 2, for pump powers between 1.4 and 2.8 W, amplification decreases significantly and deviates from the exponential increase to a more linear increase and in region 3, for pump powers above 2.8 W, amplification saturates.

Output spectra for selected values of coupled pump powers in each each of these regions, are plotted in Fig. 4.12. From the spectra, we observe that at 1.2 W pump input in region 1, only the amplified seed at 1064 nm is present in the spectrum. At 2.5 W pump input in region 2, noise is observed at around 1034 nm, however the amplified seed at 1064 nm is higher than the noise. At 3.8 W pump input in region 3, the amplified seed output is observed to be almost at the same level as for 2.5 W pump input, but the amplitude of noise is significantly higher. From the wavelength of the noise spectra, we conclude that the noise is due to ASE propagating in forward direction.

To estimate the amount of ASE in the output, a 1000 nm LPF is used instead of the 1064 nm BPF (in Fig. 4.8) and the measurements are repeated for different pump powers. The value of ASE is calculated by subtracting the amplified seed powers measured with 1064 nm BPF from the total power measured with 1000 nm LPF, taking into account the specified transmissivities. The values are plotted in Fig. 4.13.

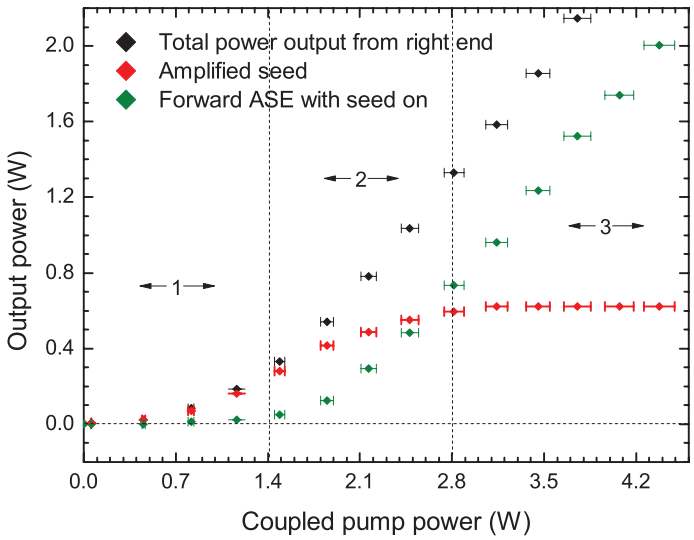

Figure 4.13: Amplified seed and ASE measurements.

From the Fig. 4.13 we observe that ASE powers are negligible in region 1. ASE increases in region 2, but is low compared to the amplified seed powers. A linear

increase in ASE powers is observed in region 3.

This indicates that even in the presence of a seed input, parasitic lasing originates from ASE at high pump powers, due to the reflectivities from fiber end facets. From the spectrum and power measurements, we conclude that the saturation observed in region 3 is due to the gain clamping resulting from onset of strong lasing in the forward propagating ASE.

The amplification measurements were repeated for a lower seed input of 3.7 mW and the outputs are plotted in Fig. 4.14, along with the 6.7 mW seed amplification outputs for comparison. For 3.7 mW seed input, the region 2 is less pronounced and gain clamping is observed for lower coupled powers (above 2.1 W) than in the case of a higher seed input. This indicates that the threshold for parasitic lasing reduces when the input seed power decreases.

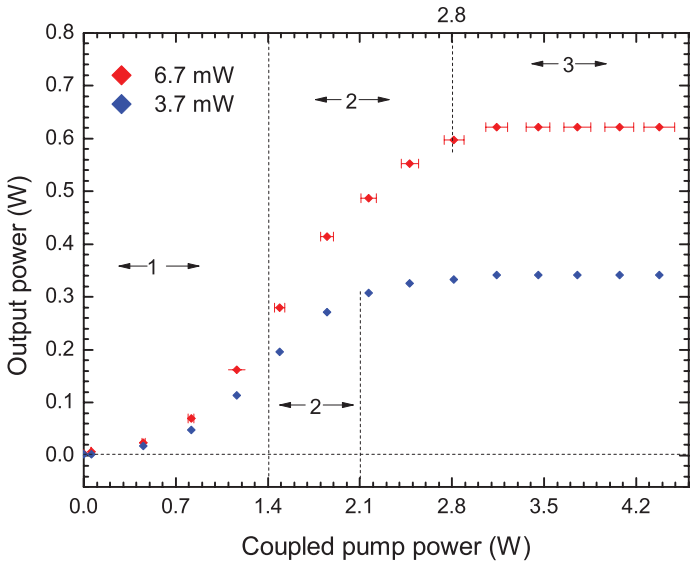

Figure 4.14: Amplified seed measurements for 6.7 mW and 3.7 mW seed input powers.

To summarize, we observe from the experimental measurements that: Strong lasing originates at ASE wavelength even due to the small reflectivities from the fiber end facets. An angle cleave (with angle $> 3^o$) reduces the reflectivity at the end facet and thus suppresses lasing in the ASE reflected from that facet. With low power seed input, exponential amplification occurs initially at low pump powers but saturates at higher pump powers when parasitic lasing at ASE wavelength becomes dominant, resulting in gain clamping. When the cleave angle at the left facet is

increased above 1^o, coupling the seed input to the low NA fiber core becomes more difficult. Hence lasing from ASE due to fiber end facet reflectivities cannot be fully avoided especially at for low input seed powers as used in the experiments.

5 Analysis

The fiber laser and amplifier devices described in the experimental sections are simulated using the RP-Fiber Power simulation software. Results of the simulation models are compared with the corresponding experimental measurements in this chapter. The effects of various design and fiber parameters are analyzed and estimated by comparing the simulation and experimental results.

5.1 Fiber laser

The backward pumped Ytterbium-doped double clad fiber laser described in section 4.3 is modeled in RP-Fiber Power simulation software. Fiber dimensions and parameters are defined according to the specifications of the Liekki Yb1200-20/125DC fiber (see Table 4.1) and the absorption and emission cross-sections provided by Liekki (see Fig. 4.1). The lasing wavelength is assumed to be 1040 nm, as observed during the experimental measurements. Four optical channels are defined in the core of the active fiber, correspondingly for propagation pump and laser light in the forward and backward directions. The pump and laser light are assumed to have radially symmetric top-hat and Gaussian transverse intensity profiles, respectively. Fluorescence life time of Yb^{3+} ions is assumed to be 0.85 ms, as provided by Liekki. The complete simulation code for the continuous wave laser model is give in Appendix 6.

Reflectivities (R_1 and R_2) of the resonator cavity are one of the most important experimental parameters affecting the performance of a linear cavity fiber laser. Particularly when the reflection from fiber end facet is used to form the resonator cavity at the output coupling end, it is difficult to estimate the exact value of reflectivity. For a perpendicularly cleaved and polished fiber end facet, the maximum reflectivity is given by the Fresnel reflection (4 %) value for air-fiber interface. In our experimental setup, the fiber facet at the left end was nearly perpendicularly cleaved but not polished. It can be expected that the reflectivity (R_1) from this fiber facet would be less than 4 %. On the right end of the fiber, an arrangement of metallic mirror with a very high, wavelength independent reflectivity (R>99 %) was used (see Fig. 4.4). Allowing for possible misalignment losses, the reflectivity on the right end (R_2) is estimated to be between 50 to 100 %. With these initial estimates, different combinations of end reflectivities are used for the simulations and the results are compared to the measurements in Fig. 5.1.

From the simulation results, the influence of end reflectivities can be summarized as: Reducing the left end reflectivity (R_1) increases the lasing threshold but has no effect on the laser slope efficiency (S1 and S2 in Fig. 5.1). Reducing the right end

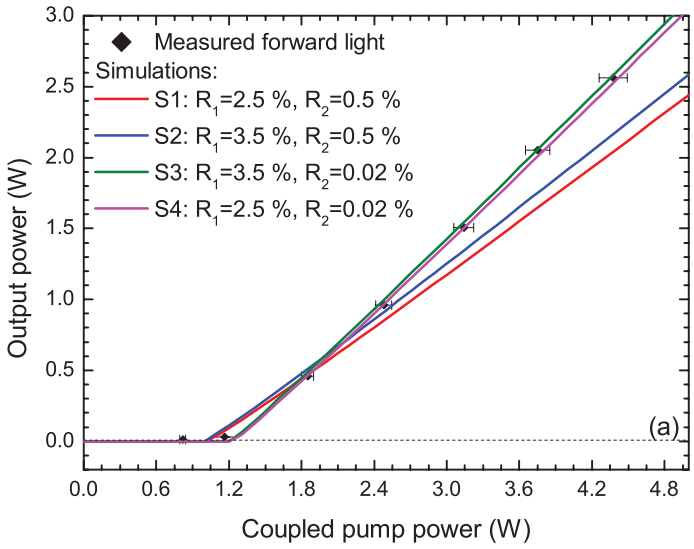

Figure 5.1: Fiber laser simulations for different reflectivities.

reflectivity (R_2) for constant R_1 not only increases the laser threshold but also reduces slope efficiency (S2 and S3). Reducing R_2 and increasing R_1 further decreases the slope efficiency but the laser threshold decreases slightly (S2 and S4).

This indicates that it is essential to have high reflectivities on both ends of the fiber laser to achieve high slope efficiency at a low threshold pump power. By comparison with measurements, the slope efficiencies are best matched for the value of R_2 close to 100 %. Whereas, best agreement between the simulated and measured laser threshold is obtained for R_1 approximately equal to 1 %. The simulation for this set of reflectivities is shown separately along with the measurements in Fig. 5.2.

By fitting the simulation result with a linear function, we estimate the slope efficiency to be 85.44 % and the lasing threshold to be 0.8 W. These values have an agreement of more than 94 %, with the values obtained from the linear fit to the measurement data (90 % and 0.815 W, respectively). Thus in the case of a Ytterbium-doped double-clad fiber laser, we find that the simulation model predicts the behavior of the experimental device very accurately.

5.2 Fiber amplifier

In the experimental analysis of the fiber amplifier setup without any seed input (section 4.4), we observed significant lasing originating in the forward and backward ASE, due to the presence of finite reflectivities at the fiber end facets. The values

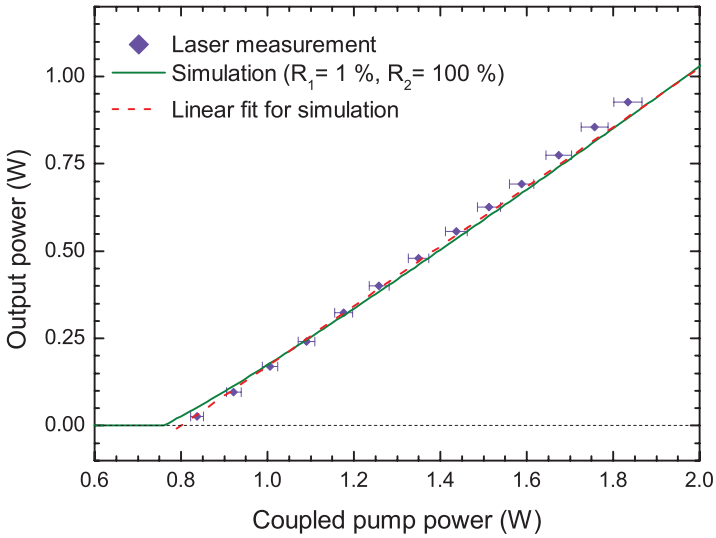

Figure 5.2: Fiber laser: simulation versus measurement.

these end reflectivities can be estimated by comparison with simulations. Hence, we first use a laser simulation model similar to the one described in section 5.1, to simulate the output powers of forward and backward light from the fiber for different sets of fiber end reflectivities.

Compared to the simulation model in section 5.1, the fiber specifications are now defined according to the values given for Yb600-20/125DC fiber (see Table 4.1). Absorption and emission cross-sections given by Liekki for the Yb1200-20/125DC fiber are also used in this case. From the cleave angles of left and right facets (1^o and 3.5^o, respectively) it is estimated that the reflectivity R_1 is higher than R_2. The forward and backward laser outputs from the simulations are plotted in Fig. 5.3 along with the corresponding measurements, for different sets of end reflectivities.

From the simulation results, the effect of end reflectivities can be summarized as: Increasing R_1 increases the slope efficiency of lasing in forward laser but decreases the slope efficiency in backward laser. The lasing threshold remain almost same in both cases (S1 and S2 in Fig. 5.1). Reducing R_2 while keeping R_1 constant again increases slope efficiency in forward laser and further decreases slope efficiency in backward laser. Also, the threshold increases slightly in both cases (S2 and S3). Reducing R_1 while keeping R_2 at the lower value however, decreases the slope efficiency in forward laser and increases the slope efficiency in backward laser while not having much effect on the thresholds (S3 and S4). However for any specific set of reflectivities, it is not possible to attain a good match between the simulation and measurements simultaneously for both forward and backward lasers.

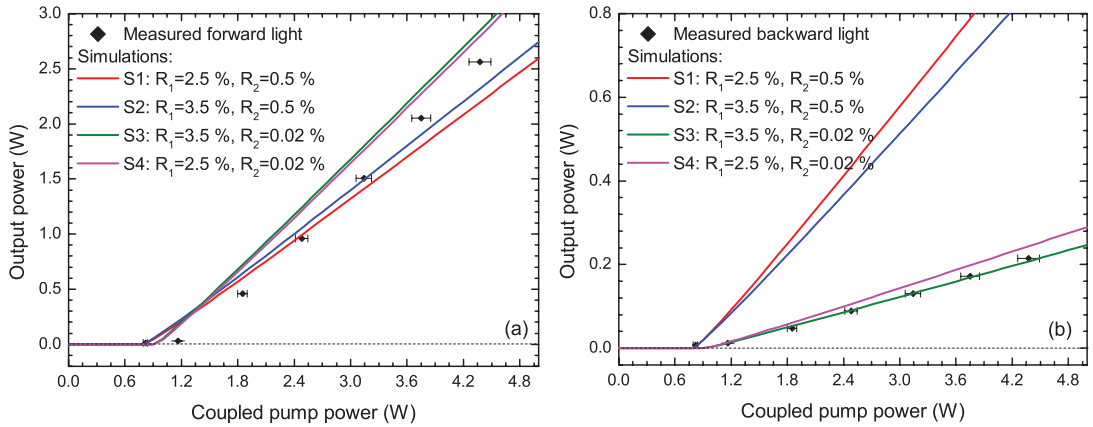

Figure 5.3: (a) Forward and (b) Backward laser simulations for different reflectivities.

In order to further study the disagreement between simulation and measurements, the amplification outputs are analyzed. For this, a continuous wave amplifier is modeled using RP-Fiber Power software by introducing a non-zero seed input. The code for this model is given in Appendix 6. Since the presence of significant ASE even with a seed input was observed in the experiments, ASE channels in the 900 to 1100 nm wavelength range are included in the amplifier simulation model in both forward and backward directions. The amplified seed outputs from the simulation model, for different sets of R_1 and R_2 and seed input of 6.7 mW are plotted in Fig. 5.4, along with the corresponding experimental measurements.

By comparing the simulation results with the measurements, we observe: Gain clamping occurs in all simulation conditions. For high values of R_2, the simulations show much lower output than measurements in the region where gain clamping is observed (region 3). By reducing R_2 and increasing R_1, the output powers in the gain clamped region can be brought closer to the measured values. For any set of reflectivities, the simulation predicts considerably higher amplification in region 1 and a sharper transition to gain clamping. These discrepancies could not be corrected by varying only the end reflectivities.

The lower powers observed in region 1 for all simulations indicate that the overall emission characteristics of the fiber are poorer than the values assumed in the simulations. The absorption and emission cross-sections for the Yb600-20/125DC fiber were not specifically measured. Therefor we study the influence of possible differences in the cross-sections by using the values presented by Paschotta *et al.*, in [37] instead of the values given by Liekki for the Yb1200 fiber. The same set

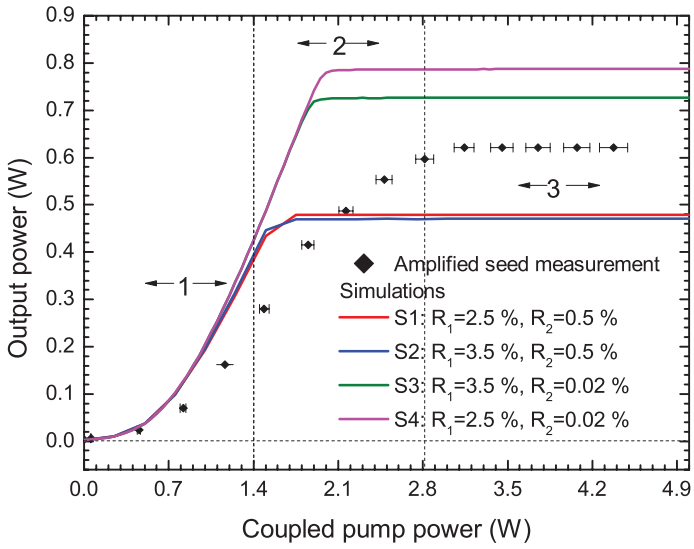

Figure 5.4: Amplified seed simulations for different reflectivities.

of simulations for forward and backward laser as well as amplified seed outputs, are repeated using the cross-sections presented by Paschotta *et al.* The results are presented in Figs. 5.5 and 5.6.

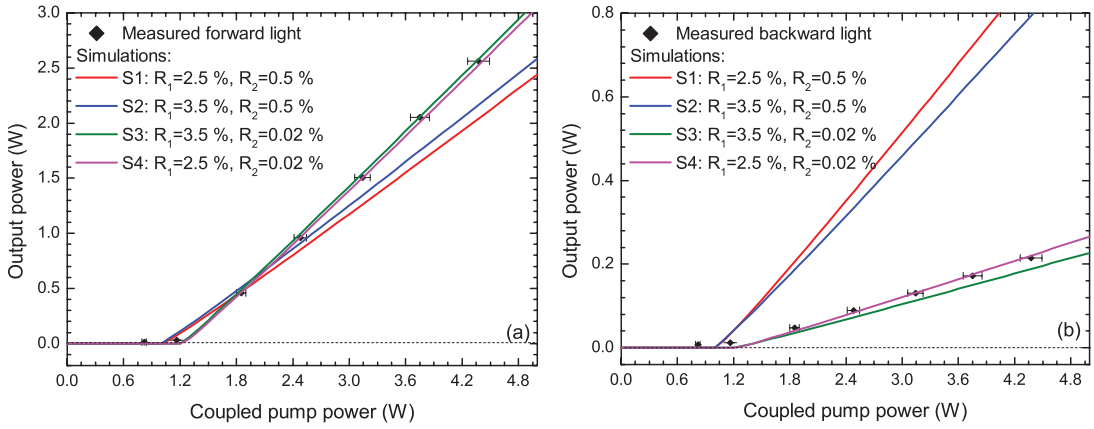

Figure 5.5: (a) Forward and (b) backward laser simulations for different reflectivities using Paschotta cross-sections.

From the simulations using fiber cross-section given in [37], we observe: Powers of the forward and backward lasers also match closely for simulations S3 and S4. Measured and simulated powers in region 1 match closely for all sets of reflectivities. Simulation S3 yields a better match with respect to the amplified seed measurements

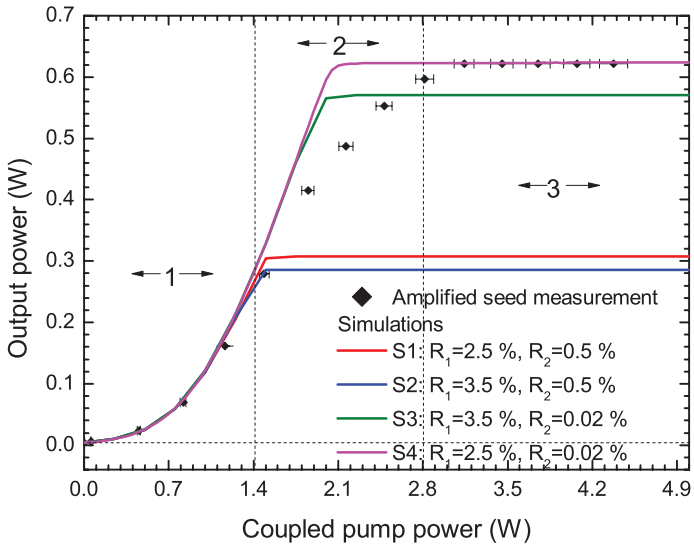

Figure 5.6: Amplified seed simulations for different reflectivities using Paschotta cross-sections.

in region 3. Thus with lower emission cross-section values in the 1000 to 1100 nm wavelength region, we observe good agreement between all measurements and simulation outputs for the values of R_1=2.5 % and R_2=0.02 %.

Based on these observations, we further compare the results of simulation S3 with other measured data. For instance, in Fig. 5.7 the measured ASE powers during amplification are compared to the simulated values. Here we observe that the simulation predicts a well defined lasing threshold at which point the gain clamping starts in the amplified output. However, in the measurements, a more gradual increase of ASE powers and corresponding decrease in amplification, were observed for coupled pump powers between 1.4 and 2.8 W. This discrepancy can be attributed to the nature of experiments.

In Fig. 5.8, the simulation results for 6.7 mW and 3.7 mW seed input are compared with the corresponding measurements. Similar results are obtained for the lower seed input, where the gain clamping occurs at a lower coupled pump power.

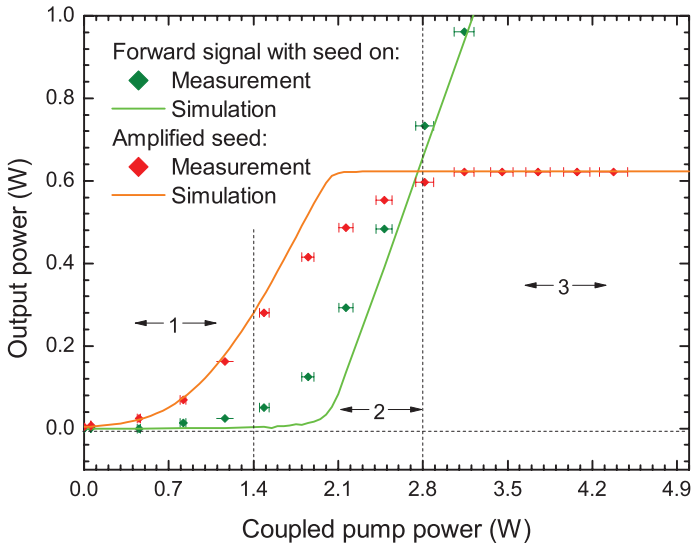

Figure 5.7: Simulation versus measurement values of FWASE and amplified output for 6.7 mW seed input.

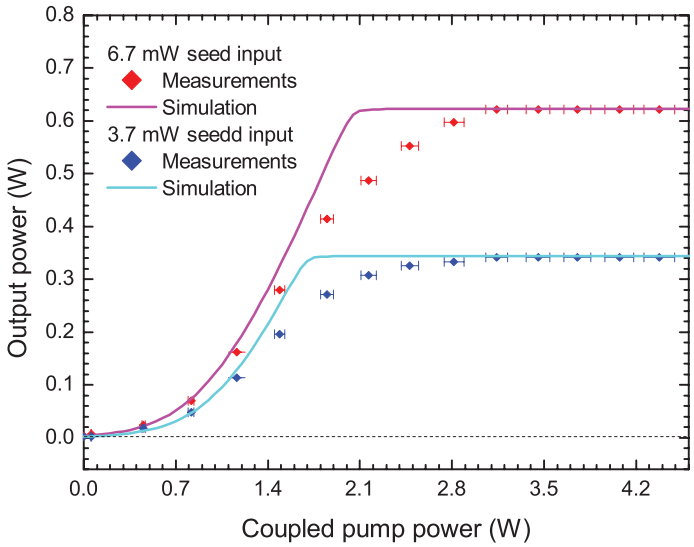

Figure 5.8: Simulation versus measurement outputs for different seed power inputs.

6 Summary

Fiber amplifiers based on Ytterbium-doped fibers are of particular interest in high-power applications due to their numerous advantages. To optimize the performance of such devices, careful analysis of the influence of a wide range of parameters is required.

In this thesis the amplification in Ytterbium-doped fibers has been studied experimentally and theoretically. For the experimental analysis, a fiber laser and an amplifier operating in the continuous wave regime, were designed based on Ytterbium-doped double-clad fibers. Theoretical studies were performed by modeling these devices using a commercial simulation software.

We built a fiber laser using a short length of highly doped active fiber, to estimate the emission characteristics of the Ytterbium-doped gain medium. The resonator cavity was realized from the Fresnel reflections of the fiber facet on the output coupling end and a highly reflective mirror on the other end. Lasing was observed at 1040 nm with a slope efficiency of 90 % corresponding to the coupled pump power.

Further a fiber amplifier was built using an active fiber with a lower doping concentration. The fiber facets were angle cleaved to reduce end reflectivities. However, for zero seed input, strong parasitic lasing originating from ASE was still observed due to the influence of the finite end reflectivities. For low seed inputs, the measurements showed three distinct amplification regimes depending on the coupled pump powers. The amplification was exponential at low pump powers, but gradually reduced at higher powers reaching a strong saturation above 2.8 W. From the power and spectra measurements, the amplification was concluded to be gain clamped due to onset of lasing in the forward propagating ASE.

For theoretical analysis, the fiber devices were modeled using the RP-Fiber Power simulation software. In the laser simulations, the slope efficiency and lasing threshold of the output powers, showed a strong dependence on the values of end reflectivities. The values were estimated by comparison with measurements. An agreement of over 94 % was obtained between simulation and experimental results in case of the fiber laser.

In the amplifier simulations, the output seed powers showed a strong dependence on not only the end reflectivities but also the fiber absorption and emission cross-sections. The values of end reflectivities influenced mostly the threshold for gain clamping, whereas the fiber cross-sections affected the overall amplified seed powers. In comparison with measured seed powers, the simulation results showed

a good agreement in the exponential and gain clamped output regimes. We have thus been able to verify that the specified simulation tool can be used to accurately describe the performance of designed fiber devices, but good knowledge of experimental parameters is needed to avoid any discrepancies.

Based on the study of Ytterbium-doped fibers and verification of the simulation tool, more complex fiber systems can further be designed. Future work involves the design and implementation of a master oscillator power amplifier (MOPA) system based on Ytterbium-doped fibers for amplification of picosecond pulses. The device shall be used as a high-power pump source for generating a supercontinuum spectrum.

References

[1] E. Snitzer, "Proposed fiber cavities for optical masers," *Journal of Applied Physics*, vol. 32, no. 1, pp. 36–39, 1961.

[2] E. Snitzer, "Neodymium glass laser," in *Quantum Electronics*, vol. 1, p. 999, 1964.

[3] C. J. Koester and E. Snitzer, "Amplification in a fiber laser," *Applied Optics*, vol. 3, no. 10, pp. 1182–1186, 1964.

[4] J. Stone and C. A. Burrus, "Neodymium-doped silica lasers in end-pumped fiber geometry," *Applied Physics Letters*, vol. 23, no. 7, pp. 388–389, 1973.

[5] J. Stone and C. Burrus, "Neodymium-doped fiber lasers: Rom temperature CW operation with an injection laser pump," *Applied Optics*, vol. 13, pp. 1256–1258, 1974.

[6] R. Mears, L. Reekie, S. Poole, and D. Payne, "Neodymium-doped silica single-mode fibre lasers," *Electronics Letters*, vol. 21, no. 17, pp. 738–740, 1985.

[7] S. Poole, D. N. Payne, and M. Fermann, "Fabrication of low-loss optical fibres containing rare-earth ions," *Electronics Letters*, vol. 21, no. 17, pp. 737–738, 1985.

[8] J. Townsend, S. Poole, and D. Payne, "Solution-doping technique for fabrication of rare-earth-doped optical fibres," *Electronics Letters*, vol. 23, no. 7, pp. 329–331, 1987.

[9] R. J. Mears, L. Reekie, I. M. Jauncey, and D. N. Payne, "Low-noise Erbium-doped fiber amplifier at 1.54 μm," *Electronics Letters*, vol. 23, no. 19, pp. 1026–1028, 1987.

[10] E. Desurvire, J. R. Simpson, and P. C. Becker, "High-gain Erbium-doped traveling-wave fiber amplifier," *Optics Letters*, vol. 12, no. 11, pp. 888–890, 1987.

[11] D. C. Hanna, R. M. Percival, I. R. Perry, R. G. Smart, P. J. Suni, J. E. Townsend, and A. C. Tropper, "Continuous-wave oscillation of a monomode Ytterbium-doped fiber laser," *Electronics Letters*, vol. 24, no. 17, pp. 1111–1113, 1988.

[12] Y. Jeong, A. J. Boyland, J. K. Sahu, S. H. Chung, J. Nilsson, and D. N. Payne, "Multi-kilowatt single-mode Ytterbium-doped large-core fiber laser," *Journal of the Optical Society of Korea*, vol. 13, no. 4, pp. 416–422, 2009.

[13] A. Bertoni and G. Reali, "A model for the optimization of double-clad fiber laser operation," *Applied Physics B*, vol. 66, pp. 547–554, 1998.

[14] Z. Duan, L. Zhang, and J. Chen, "Analytical characterization of an end pumped rare-earth-doped double-clad fiber laser," *Optical Fiber Technology*, vol. 13, no. 2, pp. 143 – 148, 2007.

[15] Z. Luo, C. Ye, G. Sun, Z. Cai, M. Si, and Q. Li, "Simplified analytic solutions and a novel fast algorithm for Yb^{3+}-doped double-clad fiber lasers," *Optics Communications*, vol. 277, no. 1, pp. 118 – 124, 2007.

[16] L. Zhang, H. Liu, and X. Li, "Theoretical analysis of Yb^{3+}-doped double-clad fiber lasers using a new analytical method," *Optik - International Journal for Light and Electron Optics*, 2012.

[17] G. Hu, C. Shan, X. Deng, J. Zhang, Y. Pan, and L. Wang, "Threshold characteristics of linear cavity Yb^{3+}-doped double-clad fiber laser," *Optics & Laser Technology*, vol. 37, no. 1, pp. 3–7, 2005.

[18] X. Liao and C. Huang, "Optimization of Yb^{3+}-doped double-clad fiber lasers using a new approximate analytical solution," *Optics & Laser Technology*, vol. 43, no. 1, pp. 55 – 61, 2011.

[19] Y.-Y. Fan, C.-C. Ye, C.-Y. Wu, and Z.-P. Cai, "High-power narrow-linewidth wavelength-tunable Yb^{3+}-doped double-clad fiber lasers," *Proceedings of SPIE*, vol. 7134, pp. 71342H–1, 2008.

[20] A. Einstein, "On the quantum theory of radiation," *Physikalische Zeitschrift*, vol. 18, pp. 121–128, 1917.

[21] J. P. Gordon, H. J. Zeiger, and C. H. Townes, "Molecular microwave oscillator and new hyperfine structure in the microwave spectrum of NH_3," *Physical Review*, vol. 95, no. 1, pp. 282–284, 1954.

[22] A. L. Schawlow and C. H. Townes, "Infrared and optical masers," *Physical Review*, vol. 112, no. 6, p. 1940, 1958.

[23] T. H. Maiman, "Stimulated optical radiation in ruby," *Nature*, vol. 187, pp. 493–494, 1960.

[24] A. C. van Heel, "A new method of transporting optical images without aberrations," *Nature*, vol. 173, p. 39, 1954.

[25] N. Wolff and R. Pressley, "Optical maser action in an Eu+3-containing organic matrix," *Applied Physics Letters*, vol. 2, no. 8, pp. 152–154, 1963.

[26] L. Johnson, "Optical maser characteristics of rare-earth ions in crystals," *Journal of Applied Physics*, vol. 34, no. 4, pp. 897–909, 1963.

[27] J. Hecht, "Optical amplifiers," *Optics & Photonics News*, 2002.

[28] A. Tünnermann, T. Schreiber, and J. Limpert, "Fiber lasers and amplifiers: an ultrafast performance evolution," *Applied optics*, vol. 49, no. 25, pp. F71–F78, 2010.

[29] E. Snitzer, H. Po, F. Hakimi, R. Tumminelli, and B. C. McCollum, "Double-clad, offset core Nd fiber laser," in *Optical Fiber Sensors*, Optical Society of America, 1988.

[30] M. H. Muendel, "Optimal inner cladding shapes for double-clad fiber lasers," in *Lasers and Electro-Optics, 1996. CLEO '96., Summaries of papers presented at the Conference on. IEEE*, p. 209, 1996.

[31] D. Kouznetsov and J. V. Moloney, "Efficiency of pump absorption in double-clad fiber amplifiers. iii. calculation of modes," *Journal of the Optical Society of America B*, vol. 19, no. 6, pp. 1304–1309, 2002.

[32] J. Knight, T. Birks, P. S. J. Russell, and D. Atkin, "All-silica single-mode optical fiber with photonic crystal cladding," *Optics Letters*, vol. 21, no. 19, pp. 1547–1549, 1996.

[33] F. D. Teodoro, M. K. Hemmat, J. Morais, and E. C. Cheung, "High peak power operation of a 100 μm-core, Yb-doped rod-type photonic crystal fiber amplifier," *Proceedings of SPIE*, vol. 7580, pp. 758006–1 – 8, 2006.

[34] J. Limpert, T. Schreiber, S. Nolte, H. Zellmer, A. Tünnermann, R. Iliew, F. Lederer, J. Broeng, G. Vienne, A. Petersson, *et al.*, "High-power air-clad large-mode-area photonic crystal fiber laser," *Optics Express*, vol. 11, no. 7, pp. 818–823, 2003.

[35] J. Limpert, N. Deguil-Robin, I. Manek-Hönninger, F. Salin, F. Röser, A. Liem, T. Schreiber, S. Nolte, H. Zellmer, A. Tünnermann, *et al.*, "High-power rod-type photonic crystal fiber laser," *Optics Express*, vol. 13, no. 4, pp. 1055–1058, 2005.

[36] J. Limpert, O. Schmidt, J. Rothhardt, T. Schreiber, A. Tünnermann, S. Ermeneux, P. Yvernault, F. Salin, *et al.*, "Extended single-mode photonic crystal fiber lasers," *Optics Express*, vol. 14, no. 7, pp. 2715–2720, 2006.

[37] R. Paschotta, J. Nilsson, A. C. Tropper, and D. C. Hanna, "Ytterbium-doped fiber amplifiers," *IEEE Journal of Quantum Electronics*, vol. 33, no. 7, pp. 1049–1056, 1997.

[38] H. M. Pask, R. J. Carman, D. C. Hanna, A. C. Tropper, C. J. Mackechnie, P. R. Barber, and J. M. Dawes, "Ytterbium-doped silica fiber lasers: versatile sources for the 1-1.2 μm region," *IEEE Journal Selected Topics in Quantum Electronics*, vol. 1, no. 1, pp. 2–13, 1995.

[39] R. Paschotta, "Encyclopedia of laser physics and technology." http://www.rp-photonics.com/encyclopedia.html.

[40] J. Nilsson, W. Clarkson, R. Selvas, J. Sahu, P. Turner, S. Alam, and A. Grudinin, "High-power wavelength-tunable cladding-pumped rare-earth-doped silica fiber lasers," *Optical Fiber Technology*, vol. 10, no. 1, pp. 5–30, 2004.

[41] R. Paschotta, J. Nilsson, P. Barber, J. Caplen, A. C. Tropper, and D. C. Hanna, "Lifetime quenching in Yb-doped fibres," *Optics Communications*, vol. 136, no. 5, pp. 375–378, 1997.

[42] C. Barnard, P. Myslinski, J. Chrostowski, and M. Kavehrad, "Analytical model for rare-earth-doped fiber amplifiers and lasers," *IEEE Journal of Quantum Electronics*, vol. 30, pp. 1817–1830, 1994.

[43] A. A. M. Saleh, R. Jopson, J. Evankow, and J. Aspell, "Modeling of gain in Erbium-doped fiber amplifiers," *IEEE Photonics Technology Letters*, vol. 2, no. 10, pp. 714–717, 1990.

[44] C. R. Giles and E. Desurvire, "Modeling Erbium-doped fiber amplifiers," *Journal of Lightwave Technology*, vol. 9, no. 2, pp. 271–283, 1991.

[45] D. Scarano, G. Ghinamo, and I. Montrosset, "Numerical simulation of DBR Erbium-doped fiber lasers," in *Photonics West'96*, pp. 156–162, International Society for Optics and Photonics, 1996.

[46] J. Chen, X. Zhu, and W. Sibbett, "Derivation of the threshold pump power of Erbium-doped fiber lasers," *Optics Letters*, vol. 17, no. 13, pp. 926–928, 1992.

[47] M. Mignon and E. Desurvire, "An analytical model for the determination of optimal output reflectivity and fiber length in Erbium-doped fiber lasers," *IEEE Photonics Technology Letters*, vol. 4, no. 8, pp. 850–852, 1992.

[48] L. M. Frantz and J. S. Nodvik, "Theory of pulse propagation in a laser amplifier," *Journal of Applied Physics*, vol. 34, no. 8, pp. 2346–2349.

[49] C. Zhou, X. Hou, S. Du, Y. Liu, and W. Chen, "Pulsed Ytterbium-doped all fiber amplifier near 1μm," *Proceedings of SPIE*, vol. 8192, pp. 819240–1–819240–6, 2011.

[50] L. Dong and M. E. Fermann, *High Power Laser Handbook - Introduction to Optical Fiber Lasers*, ch. 15. McGraw-Hill, 2011.

[51] T. S. McComb, M. C. Richardson, and M. Bass, *Handbook of Optics - High-power fiber lasers and amplifiers*, ch. 25. McGraw-Hill, 2012.

[52] D. Kliner, "kW fiber lasers," in *Optical Fiber Communication Technical Digest*, Optical Society of America, 2012.

[53] R. Paschotta, "Understanding fiber amplifiers and lasers," *Laser Technik Journal*, vol. 8, no. 5, pp. 45–47, 2011.

Appendix A

Simulation code for CW fiber laser:

```
include Units.inc

;--------------------------------------

; {Basic device parameters:}

L_f:=1.75 {fiber length}
No_z_steps:=100  {number of steps along the fiber}

;--------------------------------------

; {Parameters of the optical channels:}

l_p:=972.5 nm {pump wavelength}
dir_p:=forward {pump propagation direction}

l_s:=1040 nm {laser wavelength}

R1:=0.01 {reflectivity at left fiber end}
R2:=1 {reflectivity at right fiber end}

P_pump_in:=3000 mW {input pump power}

;----------------------------------------

; {Definition of fiber parameters:}

include "Yb-Liekki 1200-20-125DC.inc"

;----------------------------------------

; {Function for defining the model:}

def_model():=
  begin
  set_fiber(L_f, No_z_steps, 'Yb');
  for j:=1 to 10 do add_ring(r_core*(j/10), N_Yb);
```

```
  pump:=addinputchannel(P_pump_in, l_p, 'I_p', loss_p, dir_p);
  pump_ref:=addinputchannel(0, l_p,'I_p', loss_p, backward);
  signal_fw:=addinputchannel(0, l_s, 'I_s', loss_s, forward);
  signal_bw:=addinputchannel(0, l_s, 'I_s', loss_s, backward);
  set_R(signal_fw, R1, R2);
  set_R(pump, R1, R2);
  finish_fiber();
  end;
calc def_model()

;----------------------------------------

; {Display outputs in the Output window:}

show "remaining pump:     ", P_out(pump):d3:"W"
show "laser output:   ", P_out(signal_bw):d3:"W"
show "G_signal: ", sp_gain(signal_bw):d3:np:"dB"

;----------------------------------------

; {Plot laser output powers versus pump input powers:}

diagram 1:

"Laser output power"

x: 0, 2
"Pump input power (W)", @x
y: 0, 3
"Output power (W)", @y
frame
hx
hy

f: (set_P_in(pump, x); P_out(signal_bw)),
   step=5, color=blue, width=3,
   finish set_P_in(pump, P_pump_in)

;----------------------------------------
```

Appendix B

Simulation code for CW fiber amplifier with ASE:

```
include Units.inc

;---------------------------------------

; {Basic device parameters:}

L_f:=3.05 {fiber length}
No_z_steps:=100  {number of steps along the fiber}

;----------------------------------------

; {Definition of fiber parameters:}

include "Yb-Liekki 600-20-125DC.inc"

;----------------------------------------

; {Parameters of the optical channels:}

l_s1:=1064 nm {seed wavelength}
l_p1:=975.5 nm {pump wavelength}

P_pump1_bw_in:=800 mW {input pump power}
P_signal1_fw_in:=6.7 mW {input seed power}


R1:= 0.035 {reflectivity at left fiber end}
R2:= 0.0002 {reflectivity at right fiber end}

;---------------------------------------

; {Definition of ASE channels:}

l1_ASE:=910 nm
l2_ASE:=1100 nm
dl_ASE:=1 nm
NoModes_ASE:=2
```

```
defarray c_ASE_fw[l1_ASE, l2_ASE, dl_ASE]
defarray c_ASE_bw[l1_ASE, l2_ASE, dl_ASE]
P_ASE_fw(x):=sum(l:=l1_ASE to l2_ASE step dl_ASE, P(c_ASE_fw[l],x))
P_ASE_bw(x):=sum(l:=l1_ASE to l2_ASE step dl_ASE, P(c_ASE_bw[l],x))

;--------------------------------------

; {Function for defining the model:}

def_model():=
  begin
  set_fiber(L_f, No_z_steps, 'Yb');
  for j:= 1 to 10 do add_ring (r_core * (j/10), N_Yb);
  max_N:=N_Yb;
  max_r:=r_core;
  P_in_max:=0;
  P_in_max:=maxr(P_in_max, P_pump1_bw_in);
  pump1_bw:=
   addinputchannel(P_pump1_bw_in, l_p1, 'I_p1', loss_p, backward);
  pump_ref:=
   addinputchannel(0, l_p1,'I_p1', loss_p, forward);
  set_R(pump1_bw, R2, R1);
  P_in_max:=maxr(P_in_max, P_signal1_fw_in);
  signal1_fw:=
   addinputchannel(P_signal1_fw_in, l_s1, 'I_s1', loss_s, forward);
  set_R(signal1_fw, R1, R2);
  for l:=l1_ASE to l2_ASE step dl_ASE
   do begin
   c_ASE_fw[l]:=
    addASEchannel(l, dl_ASE, NoModes_ASE, 'I_ASE', 0, forward);
   c_ASE_bw[l]:=
    addASEchannel(l, dl_ASE, NoModes_ASE, 'I_ASE', 0, backward);
   set_R(c_ASE_fw[l], R1, R2);
   end;
  finish_fiber();
  end;
calc def_model()

;--------------------------------------

; {Calculation of ASE powers:}
```

```
P_ASE_max():=
  begin
  var P_max;
  P_max:=0;
  for l:=l1_ASE to l2_ASE step dl_ASE
  do begin
     P_max:=maxr(P_max, P_out(c_ASE_fw[l]));
     P_max:=maxr(P_max, P_out(c_ASE_bw[l]));
     end;
  P_max;
  end;

P_ASE_fw_out(l):=
  if l1_ASE <= l <= l2_ASE
  then P_out(c_ASE_fw[l])
P_ASE_bw_out(l):=
  if l1_ASE <= l <= l2_ASE
  then P_out(c_ASE_bw[l])
P_ASE_fw:=sum(l:=l1_ASE to l2_ASE step dl_ASE, P_out(c_ASE_fw[l]))
P_ASE_bw:=sum(l:=l1_ASE to l2_ASE step dl_ASE, P_out(c_ASE_bw[l]))
calc (G_ASE:=0; for l:=l1_ASE to l2_ASE step dl_ASE do
 G_ASE:=maxr(G_ASE, sp_gain(c_ASE_fw[l])))

;-----------------------------------------

; {Display outputs in the Output window:}

show "Output powers:"
P_pump1_bw_out:=P_out(pump1_bw)
show "Remaining pump:   ", P_pump1_bw_out:d5:"W"
P_signal1_fw_out:=P_out(signal1_fw)
show "signal1_fw: ", P_signal1_fw_out:d3:"W"
G_signal1:=sp_gain(signal1_fw)
show "G_signal1:  ", G_signal1:d3:np:"dB"
show" ASE powers------"
show "P_ASE_fw:   ", P_ASE_fw:d5:"W"
show "P_ASE_bw:   ", P_ASE_bw:d5:"W"
```